Weierstraß-Institut
für Angewandte Analysis und Stochastik

im Forschungsverbund Berlin e.V.

Preprint ISSN 0946 – 8633

Modelling of surface waves in poroelastic saturated materials by means of a two component continuum – Lecture notes

CISM Course: Surface waves in geomechanics, Udine, September 2004

Bettina Albers

submitted: 29th July 2004

Weierstrass Institute
for Applied Analysis
and Stochastics
Mohrenstr. 39
D – 10117 Berlin
Germany
E-Mail: albers@wias-berlin.de

No. 952
Berlin 2004

2000 *Mathematics Subject Classification.* 74J15, 76S05, 74L05, 74S99.

Key words and phrases. Surface waves, porous media, geophysics, numerical analysis of dispersion relation.

Edited by
Weierstraß-Institut für Angewandte Analysis und Stochastik (WIAS)
Mohrenstraße 39
10117 Berlin
Germany

Fax: + 49 30 2044975
E-Mail: preprint@wias-berlin.de
World Wide Web: http://www.wias-berlin.de/

Abstract

These lecture notes are devoted to an overview of the modelling and the numerical analysis of surface waves in two-component saturated poroelastic media. This is an extension to the part of this book by K. Wilmanski which is primarily concerned with the classical surface waves in single component media. We use the "simple mixture model" which is a simplification of the classical Biot's model for poroelastic media. Two interfaces are considered here: firstly the interface between a porous half space and a vacuum and secondly the interface between a porous halfspace and a fluid halfspace. For both problems we show how a solution can be constructed and a numerical solution of the dispersion relation can be found. We discuss the results for phase and group velocities and attenuations, and compare some of them to the high and low frequency approximations ($\omega \to \infty$, $\omega \to 0$, respectively).

For the interface porous medium/vacuum there exist in the whole range of frequencies two surface waves – a leaky Rayleigh wave and a true Stoneley wave. For the interface porous medium/fluid one more surface wave appears – a leaky Stoneley wave. For this boundary velocities and attenuations of the waves are shown in dependence on the surface permeability. The true Stoneley wave exists only in a limited range of this parameter. At the end we have a look on some results of other authors and a glance on a logical continuation of this work, namely the description of the structure and the acoustic behavior of partially saturated porous media.

Contents

1 Introduction

The classical approach to the propagation of surface waves is based on one-component elastic models (for a detailed presentation of solutions for some of such problems see e.g. [40]). At a plane boundary of a homogeneous linear elastic material solely a true Rayleigh wave appears, while at the interface of a semiinfinite elastic solid and a semiinfinite ideal fluid the Rayleigh wave is a leaky surface wave and an additional true Stoneley wave emerges. A true surface wave propagates along the surface direction and decays exponentially with depth, while leaky surface waves are attenuated in the surface direction and radiate energy into bulk or other surface waves. It is customary in the literature on waves in porous materials to call leaky surface waves pseudosurface waves (e.g. [19], [13], first used in [28]). For instance, there exist pseudo-Rayleigh, pseudo-Stoneley etc. waves. In this article we prefer to call these waves *leaky surface waves* (as e.g. done in [33]). However, the two terms possess the same meaning: *A leaky surface wave is identical with a pseudosurface wave.* It is known that surface waves in linear models result from the combination of bulk waves [37]. Physically, this means that at any point of the boundary bulk longitudinal and shear waves combine into the surface wave which must be slower than all bulk waves. In a one-component medium we have one longitudinal wave P (primary) and one transversal wave S (secondary or shear). The additional component in saturated porous media yields – compared to the one-component body – the existence

of an additional bulk wave, the $P2$-wave, and thus also to an additional surface wave which, in dependence on the interface, may be of true or leaky type. For instance, on a permeable boundary, dividing the system into a saturated poroelastic material and an ideal fluid, three surface waves appear. This is due to the fact that the system of bulk waves consists of four waves: $P1$-, $P2$-, S-waves in the poroelastic material and a P-wave in the fluid. The third surface wave is carried primarily by the fluid outside of the porous material and, consequently, its velocity is bigger than this of the $P2$-wave but smaller than the velocity of the P-wave in the fluid. Such waves are commonly observed in laboratory (e.g. [25]) and borehole experiments (e.g. [46]), their theoretical investigation within Biot's model was carried, for instance, by Norris [26].

In application to soils, the underground consists of several layers. Thus an extension of the theoretical description of wave propagation is necessary. Up to now it is done for single component materials (e.g. Lai [23], Rix *et al.* [30]) in which the soil is considered to be heterogeneous. Then, dispersion on heterogeneities is responsible for the existence of several modes of propagation each travelling at a different phase and group velocity (modal velocities). In the approximation by a layered structure dispersion arises from constructive interference phenomena (see [36]) occurring in media which are either bounded (e.g. rods plates, and other types of waveguides) or heterogeneous.

1.1 Practical aims

The theoretical investigation of surface waves in porous materials which is performed in this work is motivated by the possible construction of a method of nondestructive testing of materials. The term *nondestructive testing* denotes inspection methods which are used to investigate either the structure of a body or to search for the presence of defects without causing any effect on the properties of the medium. The notion "nondestructive testing" stands for a number of different methods like acoustics, radiography, dye penetration or magnetic particle inspection (for an introduction and examples see e.g. [24]). Nondestructive testing methods are used for many reasons such as to ensure product integrity and reliability, to prevent failure, due to often lower costs in comparison to conventional methods etc. Thus it is, for instance, possible to analyze porosity, voids, inclusions, cracks etc. Nondestructive testing is used in various areas such as, for example,

- geophysics, i.e. testing of soils and rocks,
- civil engineering, i.e. testing of concrete and other porous construction materials,
- road construction, i.e. testing of the road surface and the pavement,
- medicine, i.e. testing of bones and soft tissues,
- electronic industry, e.g. testing of surface coatings by nanomaterials.

Different operational areas require very different regions of frequencies of the waves: for field measurements in soil mechanics which are required in practical applications the range of applicable frequencies lies between 1 Hz and 100 Hz. However, this value differs considerably from laboratory measurements on such materials [39]. For soil samples the frequency region in such tests lies around some kHz. This range can be extended to some MHz for stones or concrete by the application of a laser technique [27], [21]. Medical

applications (see e.g. [22]) allow for frequencies up to approx. 3 MHz while testing of nanomaterials requires frequencies of approx. 100 MHz (see Chapter 11 of [24]).

Here, we want to focus our attention on the nondestructive testing of geomaterials by the analysis of surface waves. For this analysis one can choose two different ways in which a dynamic disturbance is excited: harmonic or impact excitation. In contrast to the far field approximation of seismic waves which is usually based on the frequency analysis, engineering applications were primarily concerned with waves initiated by chopping or explosions. This is not the case any more. Numerous experiments and measurements are made nowadays by devices producing harmonic vibrations (e.g. [30]). They show that the investigation of a problem in dependence on a real frequency ω is more adequate than a comparable analysis with a real wavelength $\frac{2\pi}{k}$ as control variable.

1.2 Theoretical background

1.2.1 Biot's model

The most popular and widespread model for the theoretical description of processes in fluid-saturated porous media is the *Biot's model.* It has been introduced by Maurice A. Biot in 1941 for a consolidation problem and was the basis for the analysis of the propagation of body waves in a two-component medium since 1956 [11]. In the notation of the present article Biot's momentum balances have the following form

$$\begin{aligned}
\rho_0^F \frac{\partial \mathbf{v}^F}{\partial t} &= \kappa \rho_0^F \operatorname{grad} \varepsilon + Q \operatorname{grad} \operatorname{tr} \mathbf{e}^S - \pi \left(\mathbf{v}^F - \mathbf{v}^S \right) + \rho_{12} \left(\frac{\partial \mathbf{v}^F}{\partial t} - \frac{\partial \mathbf{v}^S}{\partial t} \right), \qquad (1) \\
\rho_0^S \frac{\partial \mathbf{v}^S}{\partial t} &= \lambda^S \operatorname{grad} \operatorname{tr} \mathbf{e}^S + 2\mu^S \operatorname{div} \mathbf{e}^S + Q \operatorname{grad} \varepsilon + \pi \left(\mathbf{v}^F - \mathbf{v}^S \right) - \rho_{12} \left(\frac{\partial \mathbf{v}^F}{\partial t} - \frac{\partial \mathbf{v}^S}{\partial t} \right),
\end{aligned}$$

where $\mathbf{v}^F, \mathbf{v}^S$ denote the macroscopic (average) partial velocities of the fluid and of the skeleton, respectively, $\mathbf{e}^S$ is the symmetric Almansi-Hamel tensor of small deformations of the skeleton, ε is the volume change of the fluid. These quantities fulfil the following relations

$$\begin{aligned}
&\frac{\partial \mathbf{e}^S}{\partial t} = \operatorname{sym} \operatorname{grad} \mathbf{v}^S, \quad \frac{\partial \varepsilon}{\partial t} = \operatorname{div} \mathbf{v}^F, \\
&\varepsilon := \frac{\rho_0^F - \rho^F}{\rho_0^F}, \quad \zeta := n_0 (\operatorname{tr} \mathbf{e}^S - \varepsilon); \qquad (2)
\end{aligned}$$

the latter is the change of fluid contents commonly used as a field in Biot's model instead of ε. Relations (2) yield the existence of partial displacement fields $\mathbf{u}^S \equiv \mathbf{u}$, $\mathbf{u}^F \equiv \mathbf{U}$, with

$$\mathbf{e}^S = \operatorname{sym} \operatorname{grad} \mathbf{u}, \quad \mathbf{v}^S = \frac{\partial \mathbf{u}}{\partial t}, \quad \varepsilon = \operatorname{div} \mathbf{U}, \quad \mathbf{v}^F = \frac{\partial \mathbf{U}}{\partial t}. \qquad (3)$$

The quantities $\rho_0^F = n_0 \rho_0^{FR}, \quad \rho_0^S = (1 - n_0)\, \rho_0^{SR}$ denote constant (initial) mass densities, ρ_0^{FR}, ρ_0^{SR} are the initial true mass densities, n_0 is the initial porosity. The material parameters $\lambda^S, \mu^S, \kappa, Q, \pi, \rho_{12}$ are assumed to be constant. The parameter Q describes the coupling of partial stresses in the Biot's model, while ρ_{12} is attributed to the tortuosity a.

A typical simplified relation among those quantities was proposed by Berryman in 1980 (e.g. Bourbié *et al.* [12]) and has the form

$$\rho_{12} = \rho^F (1-a), \quad a = \frac{1}{2}\left(\frac{1}{n_0}+1\right). \tag{4}$$

The permeability coefficient π contains an overall information on the morphology of the porous material which includes porosity, tortuosity, viscosity of the real pore fluid etc. The form of this dependence is not needed in this work.

1.2.2 Simple mixture model

In our analysis we rely on a simpler model than this of Biot. We neglect two effects:

- the added mass effect reflected in the Biot's model by off-diagonal contributions to the matrix of partial mass densities (the parameter ρ_{12}),
- the static coupling effect between partial stresses (the parameter Q).

The first contribution is neglected because it yields a non-objectivity of Biot's equations [43]. This does not mean that the tortuosity may not have an influence on the propagation of surface waves but solely that it is not well modelled by Biot. For details concerning this question see [41].

The second contribution – coupling of partial stresses Q – is neglected because it yields solely *quantitative* corrections without changing the *qualitative* behavior of the system, at least in the range of a relatively high stiffness of the skeleton in comparison with the fluid. This has been analyzed for bulk waves in [3].

Bearing the above remarks in mind it seems to be appropriate to rely on the simplified model ("simple mixture model" in which $Q = 0$, $\rho_{12} = 0$) which, in turn, reduces essentially technical difficulties.

We present here the linear form of the "simple mixture" model for a two-component poroelastic saturated medium (for details see: [44]).

Within this model the process is described by the *macroscopic* fields $\rho^F(\mathbf{x},t)$ – partial mass density of the fluid, $\mathbf{v}^F(\mathbf{x},t)$ – velocity of the fluid, $\mathbf{v}^S(\mathbf{x},t)$ – velocity of the skeleton, $\mathbf{e}^S(\mathbf{x},t)$ – symmetric tensor of small deformations of the skeleton and the porosity n. These fields satisfy the following set of linear equations

$$\begin{aligned}
&\frac{\partial \rho^F}{\partial t} + \rho_0^F \operatorname{div} \mathbf{v}^F = 0, \quad \left|\tfrac{\rho^F - \rho_0^F}{\rho_0^F}\right| \ll 1,\\
&\rho_0^F \frac{\partial \mathbf{v}^F}{\partial t} + \kappa \operatorname{grad} \rho^F + \beta \operatorname{grad}(n - n_E) + \hat{\mathbf{p}} = 0, \quad \hat{\mathbf{p}} := \pi\left(\mathbf{v}^F - \mathbf{v}^S\right),\\
&\rho_0^S \frac{\partial \mathbf{v}^S}{\partial t} - \operatorname{div}\left(\lambda^S \left(\operatorname{tr}\mathbf{e}^S\right)\mathbf{1} + 2\mu \mathbf{e}^S + \beta(n - n_E)\mathbf{1}\right) - \hat{\mathbf{p}} = 0,\\
&\frac{\partial \mathbf{e}^S}{\partial t} = \operatorname{sym}\operatorname{grad}\mathbf{v}^S, \quad \left\|\mathbf{e}^S\right\| \ll 1, \quad n_E := n_0\left(1 + \delta \operatorname{tr}\mathbf{e}^S\right),\\
&\frac{\partial (n - n_E)}{\partial t} + \Phi \operatorname{div}\left(\mathbf{v}^F - \mathbf{v}^S\right) + \frac{n - n_E}{\tau_n} = 0, \quad \left|\tfrac{n - n_0}{n_0}\right| \ll 1.
\end{aligned} \tag{5}$$

As before ρ_0^F, ρ_0^S, n_0 denote constant reference values of partial mass densities, and porosity, respectively, and $\kappa, \lambda^S, \mu^S, \beta, \pi, \tau_n, \delta, \Phi$ are constant material parameters. The first one describes the macroscopic compressibility of the fluid component, the next two are macroscopic elastic constants of the skeleton, β is the coupling constant, π is the coefficient of bulk permeability, τ_n is the relaxation time of porosity and δ, Φ describe equilibrium and nonequilibrium changes of porosity, respectively. For the purpose of this work we assume $\beta = 0$. Then the problem of evolution of porosity described by equation $(5)_5$ can be solved separately from the rest of the problem and does not influence the propagation of acoustic waves in the medium. The norm of the deformation tensor $\left\|\mathbf{e}^S\right\|$ is understood as the maximum absolute value of eigenvalues of $\mathbf{e}^S$ (the maximum stretch).

In this article we present the *simple mixture model* in order to investigate the dispersion relation for surface waves on impermeable and permeable boundaries of a fluid saturated poroelastic medium in the *whole range* of frequencies. The problem of the frequency dependence for intermediate frequencies has been widely ignored in the literature due to numerical difficulties within the Biot's model. Many numerical results were not published yet elsewhere.

1.2.3 Boundary conditions

In order to determine surface waves in a saturated poroelastic medium we need conditions for $z = 0$. The most general case which we are going to consider is the interface between a saturated porous material and an ideal fluid. Boundary conditions for such an interface were formulated by Deresiewicz & Skalak [16]. We quote them here in a slightly modified form. If we denote quantities outside of the porous medium by a "+" sign the boundary conditions have the form

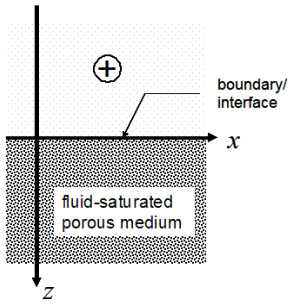

Fig. 1: Contact of a porous halfspace with an exterior.

$$
\begin{aligned}
&\bullet \quad \left(T_{13} - T_{13}^{+}\right)\big|_{z=0} \equiv T_{13}^{S}\big|_{z=0} = c_S^2 \rho_0^S \left(\frac{\partial u_1^S}{\partial z} + \frac{\partial u_3^S}{\partial x}\right)\Bigg|_{z=0} = 0,\\
&\bullet \quad \left(T_{33} - T_{33}^{+}\right)\big|_{z=0} \equiv \left(T_{33}^{S} + p^{F+} - p^{F}\right)\big|_{z=0} = \\
&\qquad = c_{P1}^2 \rho_0^S \left(\frac{\partial u_1^S}{\partial x} + \frac{\partial u_3^S}{\partial z}\right) - 2c_S^2 \rho_0^S \frac{\partial u_1^S}{\partial x} + \\
&\qquad + c_+^2 \left(\rho^{F+} - \rho_0^{F+}\right) - c_{P2}^2 \left(\rho^F - \rho_0^F\right)\big|_{z=0} = 0, \qquad (6)\\
&\bullet \quad \rho_0^F \frac{\partial}{\partial t}\left(u_3^F - u_3^S\right)\Bigg|_{z=0} = \rho_0^{F+} \frac{\partial}{\partial t}\left(u_3^{F+} - u_3^S\right)\Bigg|_{z=0},\\
&\bullet \quad \rho_0^F \frac{\partial}{\partial t}\left(u_3^F - u_3^S\right) + \alpha\left(p^F - n_0 p^{F+}\right)\Bigg|_{z=0} = 0,
\end{aligned}
$$

where u_1^S, u_3^S are x-, and z-components of the displacement $\mathbf{u}^S$, respectively, and u_3^F, u_3^{F+} are z-components of the displacements $\mathbf{u}^F$ and $\mathbf{u}^{F+}$, respectively. Simultaneously,

$$c_{P1}^2 := \frac{\lambda^S + 2\mu^S}{\rho_0^S}, \quad c_S^2 := \frac{\mu^S}{\rho_0^S}, \quad c_{P2}^2 := \kappa, \quad c_+^2 := \kappa^+, \tag{7}$$

are squares of the front velocities of the bulk waves in the porous material: $P1$ (fast wave), S (shear wave), $P2$ (slow wave, also called Biot's wave), and of the P-wave in the fluid, respectively. In the case of Biot's model there would be an additive contribution in the numerator of c_{P1} of the coupling parameter Q which is of the order of a few percent of λ^S (see: Albers, Wilmanski [3] for a detailed analysis).

The first two conditions of (6) describe the continuity of the full traction, $\mathbf{t} := \left(\mathbf{T}^S + \mathbf{T}^F\right)\mathbf{n}$, $\mathbf{n} = (0,0,1)^T$, on the boundary (i.e. momentum balance); the third condition is the continuity of the fluid mass flux (i.e. mass balance), and the last condition specifies the mass transport through the surface. The in- and outflow through the boundary is assumed to be proportional to the difference of the pore pressures on both sides of the boundary. In this condition α denotes a surface permeability coefficient (it corresponds to $\frac{1}{T}$ in the work of Feng and Johnson [19]) and p^{F+} is the external pressure. This condition relies on the assumption that the pore pressure p and the partial pressure p^F satisfy the relation $p^F \approx n_0 p$ at least in a small vicinity of the surface. For a justification of this condition it would be necessary to consider a boundary layer in the limit of zero thickness.

Some words are appropriate to explain the notion of *surface permeability*. As we see in the neighbouring figure the flow of the fluid is "straight" both outside the porous medium and inside the channels of the porous medium. However, at the entrance to the porous medium the flow is disturbed: the fluid has to find its way through the voids between the solid particles. In principle we consider a flow which is perpendicular to the boundary but in a small boundary layer it deviates from this direction. The more complicated the structure of the boundary the bigger is the resistance against the inflow and the smaller is the surface permeability parameter α. The value $\alpha = 0$ corresponds to a sealed pore situation, for $\alpha = \infty$ the boundary is completely open.

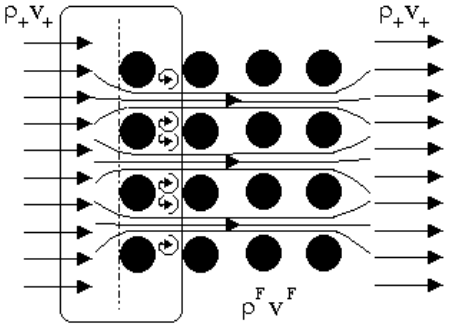

Fig. 2: Sketch of the flow into and out of a porous medium.

For the impermeable boundary with vacuum ($\alpha = 0$ in our notation, $T \to \infty$ in the work [19]), the above boundary conditions simplify to the following ones

- $$T_{13}|_{z=0} \equiv T_{13}^S\big|_{z=0} = c_S^2 \rho_0^S \left(\frac{\partial u_1^S}{\partial z} + \frac{\partial u_3^S}{\partial x}\right)\Big|_{z=0} = 0, \tag{8}$$
- $$T_{33}|_{z=0} \equiv (T_{33}^S - p^F)\big|_{z=0} = \\ = c_{P1}^2 \rho_0^S \left(\frac{\partial u_1^S}{\partial x} + \frac{\partial u_3^S}{\partial z}\right) - 2c_S^2 \rho_0^S \frac{\partial u_1^S}{\partial x} + \\ -c_{P2}^2 \left(\rho^F - \rho_0^F\right)\big|_{z=0} = 0, \tag{9}$$
- $$\frac{\partial}{\partial t}\left(u_3^F - u_3^S\right)\Big|_{z=0} = 0, \tag{10}$$

due to the fact that the quantities outside of the porous medium are equal to zero. Then the third and the fourth boundary conditions are identical.

The sealed boundary between the porous medium and a fluid yields three conditions as well but in this case there is a right hand side in relation for normal stresses.

2 Analysis by means of the "simple mixture model" – boundary porous medium/vacuum

The procedure and the numerical results for phase velocities and attenuations for this boundary are also presented in [4].

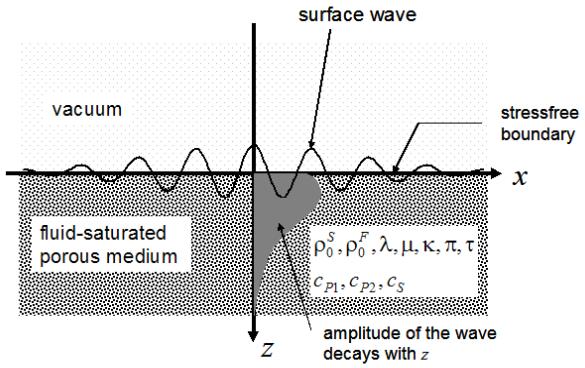

Fig. 3: Geometry of the boundary porous medium/vacuum.

2.1 Construction of solution for a semiinfinite medium

We follow here the same procedure of construction of solutions as in the works Wilmanski [42], Edelman, Wilmanski [18] and Wilmanski, Albers [45]. While in [18] an asymptotic analysis of the high-frequency properties of surface waves in function of the wavelength $1/k$ (k – wave number) within the simple mixture model was carried out, here, we consider monochromatic waves with a given *real frequency* ω. This may be considered either as a Fourier component of the expansion of the solution in time space or as a far field boundary value problem with a harmonic surface source of waves.

This choice of the description seems to be better justified from the physical point of view than the choice of the wave number, k, or, equivalently, of the wave length, $\frac{1}{k}$. In contrast to the latter case, a monochromatic wave of a given frequency, ω, can be easily induced in real field experiments. It should be mentioned, however, that these two approaches are not equivalent from the formal point of view. For an explanation of this statement see the example to the linear wave equation with damping describing longitudinal vibrations of a rod in the chapter of K. Wilmanski in this book [40]. This example is simpler but has the same structure as the problem considered in this article. The analysis in terms of real k yields, indeed, a critical behavior as shown in this example. This has been observed for Biot's wave ($P2$-wave) by I. Edelman [17]. However, according to the above remarks this observation seems to be solely of an academic interest.

2.1.1 Compatibility with field equations

We introduce the displacement vector $\mathbf{u}^S$ for the skeleton, and formally the displacement vector $\mathbf{u}^F$ for the fluid. The latter is introduced solely for the technical symmetry of

considerations and does not have any direct physical bearing. Then we have according to Helmholtz's Theorem

$$\begin{aligned} \mathbf{u}^S &= \operatorname{grad}\varphi^S + \operatorname{rot}\boldsymbol{\psi}^S, \quad \mathbf{v}^S = \frac{\partial \mathbf{u}^S}{\partial t}, \quad \mathbf{e}^S = \operatorname{sym}\operatorname{grad}\mathbf{u}^S, \\ \mathbf{u}^F &= \operatorname{grad}\varphi^F + \operatorname{rot}\boldsymbol{\psi}^F, \quad \mathbf{v}^F = \frac{\partial \mathbf{u}^F}{\partial t}. \end{aligned} \tag{11}$$

This means in coordinates

$$u_i^F = \frac{\partial \varphi^F}{\partial x^i} + \varepsilon_{ijk}\frac{\partial \psi_k^F}{\partial x^j}, \quad u_i^S = \frac{\partial \varphi^S}{\partial x^i} + \varepsilon_{ijk}\frac{\partial \psi_k^S}{\partial x^j}, \tag{12}$$

where ε_{ijk} is the permutation symbol

$$\varepsilon_{ijk} = \begin{cases} 0 & \text{for } i=j, j=k, k=i \\ 1 & \text{for } (i,j,k) \in \{(1,2,3),(2,3,1),(3,1,2)\} \\ -1 & \text{for } (i,j,k) \in \{(1,3,2),(3,2,1),(2,1,3)\} \end{cases}.$$

For the two-dimensional case[a] we make the following ansatz for monochromatic wave solutions in the x-direction

$$\begin{aligned} \varphi^S &= A^S(z)\exp\left[i\left(kx-\omega t\right)\right], \quad \varphi^F = A^F(z)\exp\left[i\left(kx-\omega t\right)\right], \\ \psi_y^S &= B^S(z)\exp\left[i\left(kx-\omega t\right)\right], \quad \psi_y^F = B^F(z)\exp\left[i\left(kx-\omega t\right)\right], \\ \psi_x^S &= \psi_z^S = \psi_x^F = \psi_z^F = 0, \end{aligned} \tag{13}$$

and

$$\rho^F - \rho_0^F = A_\rho^F(z)\exp\left[i\left(kx-\omega t\right)\right]. \tag{14}$$

We investigate the approximation of a very large relaxation time of porosity ($\tau_n \to \infty$) compared to the inverse of characteristic frequencies. This is justified in applications to soils where viscous effects related to porosity do not seem to appear. Then the nonequilibrium porosity n is determined by volume changes of the skeleton and of the fluid: $n = n_E + \Phi\left(\operatorname{tr}\mathbf{e}^S - \varepsilon\right)$. Consequently, they do not give any independent contribution to the wave problem.
Substitution in field equations (see: (5))

$$\begin{aligned} &\frac{\partial \rho^F}{\partial t} + \rho_0^F \operatorname{div}\left(\frac{\partial \mathbf{u}^F}{\partial t}\right) = 0, \qquad \mathbf{e}^S = \operatorname{sym}\operatorname{grad}\mathbf{u}^S, \\ &\rho_0^F \frac{\partial^2 \mathbf{u}^F}{\partial t^2} + \kappa \operatorname{grad}\rho^F + \pi\left(\frac{\partial \mathbf{u}^F}{\partial t} - \frac{\partial \mathbf{u}^S}{\partial t}\right) = 0, \\ &\rho_0^S \frac{\partial^2 \mathbf{u}^S}{\partial t^2} - \operatorname{div}\left(\lambda^S\left(\operatorname{tr}\mathbf{e}^S\right)\mathbf{1} + 2\mu\mathbf{e}^S\right) - \pi\left(\frac{\partial \mathbf{u}^F}{\partial t} - \frac{\partial \mathbf{u}^S}{\partial t}\right) = 0. \end{aligned} \tag{15}$$

leads after straightforward calculations[b] to the following compatibility conditions

$$B^F = \frac{i\pi}{\rho_0^F\omega + i\pi}B^S, \qquad A_\rho^F = -\rho_0^F\left(\frac{d^2}{dz^2} - k^2\right)A^F, \tag{16}$$

from momentum balance for the fluid in z-direction — from mass balance for the fluid

[a] Under this assumption of plane wave motion we are not able to describe the geometrical dispersion of waves which is the main practical motivation for applications of surface waves rather than bulk waves.

[b] $\operatorname{div}\mathbf{u}_{\text{transversal}} \equiv \operatorname{div}\operatorname{rot}\boldsymbol{\psi} \equiv \mathbf{0}$,
$\operatorname{rot}\mathbf{u}_{\text{longitudinal}} \equiv \operatorname{rot}\operatorname{grad}\varphi \equiv 0$.

as well as

$$\left[\kappa\left(\frac{d^2}{dz^2}-k^2\right)+\omega^2\right]A^F+\frac{i\pi}{\rho_0^F}\omega\left(A^F-A^S\right)=0, \tag{17}$$

from momentum balance for the fluid in x-direction

$$\left[\frac{\lambda^S+2\mu^S}{\rho_0^S}\left(\frac{d^2}{dz^2}-k^2\right)+\omega^2\right]A^S-\frac{i\pi}{\rho_0^S}\omega\left(A^F-A^S\right)=0, \tag{18}$$

from momentum balance for the skeleton in x-direction

$$\left[\frac{\mu^S}{\rho_0^S}\left(\frac{d^2}{dz^2}-k^2\right)+\omega^2+\frac{i\pi\rho_0^F}{\rho_0^S\left(\rho_0^F\omega+i\pi\right)}\omega^2\right]B^S=0. \tag{19}$$

from momentum balance for the skeleton in z-direction

2.1.2 Dimensionless notation

It is convenient to introduce a dimensionless notation. Therefore we define the following dimensionless quantities

$$\begin{aligned} &c_s:=\frac{c_S}{c_{P1}}<1, \quad c_f:=\frac{c_{P2}}{c_{P1}}, \quad \pi':=\frac{\pi\tau}{\rho_0^S}>0, \\ &r:=\frac{\rho_0^F}{\rho_0^S}<1, \qquad z':=\frac{z}{c_{P1}\tau}, \quad k':=kc_{P1}\tau, \quad \omega':=\omega\tau, \end{aligned} \tag{20}$$

where τ is an arbitrary reference time. It may be chosen as $\tau=\frac{\rho_0^S}{\pi}$ which would lead to $\pi'=1$, or it may be identical with the relaxation time of porosity τ_n. Further, we make an arbitrary choice of this normalization parameter.

2.1.3 Ansatz

For simplicity we further omit the prime in (20). Substitution of these quantities in equations (17), (18), (19) yields

$$\begin{aligned} \left[c_f^2\left(\frac{d^2}{dz^2}-k^2\right)+\omega^2\right]A^F+i\frac{\pi}{r}\omega\left(A^F-A^S\right) &= 0, \\ \left[\left(\frac{d^2}{dz^2}-k^2\right)+\omega^2\right]A^S-i\pi\omega\left(A^F-A^S\right) &= 0, \\ \left[c_s^2\left(\frac{d^2}{dz^2}-k^2\right)+\omega^2+\frac{i\pi\omega^2}{\omega+i\frac{\pi}{r}}\right]B^S &= 0. \end{aligned} \tag{21}$$

The matrix of coefficients for homogeneous materials is independent of z. Hence the differential eigenvalue problem can be easily solved. Consequently, we seek solutions in the form

$$A^F=A_f^1e^{\gamma_1 z}+A_f^2e^{\gamma_2 z}, \quad A^S=A_s^1e^{\gamma_1 z}+A_s^2e^{\gamma_2 z}, \quad B^S=B_se^{\zeta z}. \tag{22}$$

Substitution in (21) yields relations for the exponents in the form

$$\left(\frac{\zeta}{k}\right)^2 = 1 - \frac{1}{c_s^2}\left(1 + \frac{i\pi}{\omega + i\frac{\pi}{r}}\right)\left(\frac{\omega}{k}\right)^2, \tag{23}$$

$$\Rightarrow \quad \boxed{\frac{\zeta_{1,2}}{k} = \pm\sqrt{1 - \frac{1}{c_s^2}\left(1 + \frac{i\pi}{\omega + i\frac{\pi}{r}}\right)\left(\frac{\omega}{k}\right)^2},} \tag{24}$$

and

$$c_f^2\left[\left(\frac{\gamma}{k}\right)^2 - 1\right]^2 + \left[1 + \left(1 + \frac{1}{r}\right)\frac{i\pi}{\omega}\right]\left(\frac{\omega}{k}\right)^4 + \\ + \left[1 + c_f^2 + \left(c_f^2 + \frac{1}{r}\right)\frac{i\pi}{\omega}\right]\left[\left(\frac{\gamma}{k}\right)^2 - 1\right]\left(\frac{\omega}{k}\right)^2 = 0, \tag{25}$$

$$\Rightarrow \quad \boxed{\begin{aligned}\frac{\gamma_{1,2,3,4}}{k} = \pm\sqrt{1 - \frac{1}{2c_f^2}\left[\left(1 + c_f^2\right)\left(\frac{\omega}{k}\right)^2 + \left(c_f^2 + \tfrac{1}{r}\right)\tfrac{i\pi\omega}{k^2}\right] \pm} \\ \pm\sqrt{\left(\frac{\omega}{k}\right)^4\left[\frac{1}{4c_f^4}\left(1 + c_f^2\right)^2 - \tfrac{1}{c_f^2}\right] + \tfrac{i\pi}{k}\left(\frac{\omega}{k}\right)^3\left[\frac{1}{2c_f^4}\left(1 + c_f^2\right)\left(c_f^2 + \tfrac{1}{r}\right) - \right.} \\ \left. - \frac{1}{c_f^2}\left(1 + \tfrac{1}{r}\right)\right] - \frac{\pi^2\omega^2}{4c_f^4k^4}\left(c_f^2 + \tfrac{1}{r}\right)^2.\end{aligned}}$$

Simultaneously, we obtain for the eigenvectors the following relations

$$\mathbf{R}^1 = \left(B_s, A_s^1, A_f^1\right)^T, \quad \mathbf{R}^2 = \left(B_s, A_s^2, A_f^2\right)^T, \tag{26}$$

where

$$A_f^1 = \delta_f A_s^1, \quad A_s^2 = \delta_s A_f^2, \tag{27}$$

$$\delta_f := \frac{1}{r}\frac{\frac{i\pi}{\omega}\frac{\omega^2}{k^2}}{c_f^2\left[\left(\frac{\gamma_1}{k}\right)^2 - 1\right] + \left(\frac{\omega}{k}\right)^2 + \frac{i\pi}{\omega r}\frac{\omega^2}{k^2}}, \tag{28}$$

$$\delta_s := \frac{\frac{i\pi}{\omega}\frac{\omega^2}{k^2}}{\left(\frac{\gamma_2}{k}\right)^2 - 1 + \left(\frac{\omega}{k}\right)^2 + \frac{i\pi}{\omega}\frac{\omega^2}{k^2}}. \tag{29}$$

The above solution for the exponents still leaves three unknown constants B_s, A_f^2, A_s^1 which must be specified from boundary conditions.

Complex values of $\zeta_{1,2}$ and $\gamma_{1,2,3,4}$ result from the dissipation caused by the relative motion, i.e. the influence of the permeability π. As a consequence, solutions decay in z-direction but, simultaneously, they vibrate (see: Fig. 4).

2.1.4 Dispersion relation

Substitution of the above results in the boundary conditions (8)-(10) yields the following equations for the three unknown constants B_s, A_f^2 and A_s^1

$$\mathbf{AX} = \mathbf{0}, \tag{30}$$

where

$$\mathbf{A} := \begin{pmatrix} \left(\frac{\zeta}{k}\right)^2 + 1 & 2i\frac{\gamma_2}{k}\delta_s & 2i\frac{\gamma_1}{k} \\ -2ic_s^2\frac{\zeta}{k} & \left[\left(\frac{\gamma_2}{k}\right)^2 - 1 + 2c_s^2\right]\delta_s + \\ & +rc_f^2\left[\left(\frac{\gamma_2}{k}\right)^2 - 1\right] & \left(\frac{\gamma_1}{k}\right)^2 - 1 + 2c_s^2 + \\ & & +rc_f^2\left[\left(\frac{\gamma_1}{k}\right)^2 - 1\right]\delta_f \\ i\frac{r\omega}{r\omega + i\pi} & -\left(\delta_s - 1\right)\frac{\gamma_2}{k} & \left(\delta_f - 1\right)\frac{\gamma_1}{k} \end{pmatrix}, \tag{31}$$

$$\mathbf{X} := \left(\; B_s, \quad A_f^2, \quad A_s^1 \; \right)^T.$$

This homogeneous set yields the *dispersion relation:* $\det \mathbf{A} = 0$ determining the $\omega - k$ relation. The wave number k is complex for two reasons: the first one is the dissipation due to diffusion which is always present for $\pi \neq 0$ and the second is the loss of energy in leaky waves independently of π.
We investigate the numerical solution of the dispersion relation and compare the results for high and low frequencies with approximations shown in Wilmanski, Albers [45]. These are briefly summarized in the next subsection.

2.1.5 High and low frequency approximations

High frequencies In the limit $\omega \to \infty$ we immediately obtain from relations (23) and (25)

$$\left(\frac{\zeta}{k}\right)^2 = 1 - \frac{1}{c_s^2}\left(\frac{\omega}{k}\right)^2,$$
$$\left(\frac{\gamma_1}{k}\right)^2 = 1 - \left(\frac{\omega}{k}\right)^2, \quad \left(\frac{\gamma_2}{k}\right)^2 = 1 - \frac{1}{c_f^2}\left(\frac{\omega}{k}\right)^2, \tag{32}$$

and

$$\delta_f = \delta_s = 0 \quad \Rightarrow \quad \mathbf{R}^1 = \left(B_s, A_s^1, 0\right)^T, \quad \mathbf{R}^2 = \left(B_s, 0, A_f^2\right)^T. \tag{33}$$

Hence, the exponents are *real* in this limit, i.e. there appear no vibrations in z-direction. The dispersion relation follows in the form

$$\mathcal{P}_R\sqrt{1 - c_f^2\left(\frac{\omega}{k}\right)^2} + \frac{r}{c_s^4}\left(\frac{\omega}{k}\right)^4\sqrt{1 - \left(\frac{\omega}{k}\right)^2} = 0, \tag{34}$$

where

$$\mathcal{P}_R := \left(2 - \frac{1}{c_s^2}\left(\frac{\omega}{k}\right)^2\right)^2 - 4\sqrt{1 - \left(\frac{\omega}{k}\right)^2}\sqrt{1 - \frac{1}{c_s^2}\left(\frac{\omega}{k}\right)^2}. \tag{35}$$

For $r = 0$ the relation (34) reduces to $\mathcal{P}_R = 0$ which is the Rayleigh dispersion relation for single component continua. The high frequency limit, described by (34), exists for any choice of material parameters in contrast to results of Feng and Johnson [19]. The range of nonexistence of this wave related to small values of the longitudinal frame modulus, corresponding to $\mu^S < \rho^S\kappa$ in our notation, has not been investigated within the simple mixture model.

Low frequencies For the limit $\omega \to 0$ one arrives at the following results for the first order approximation of exponents (notice a singularity of the last contribution to $\frac{\gamma_2}{k}$!)

$$\left(\frac{\zeta}{k}\right)^2 = 1 - \frac{r+1}{c_s^2}\left(\frac{\omega}{k}\right)^2, \qquad \left(\frac{\gamma_1}{k}\right)^2 = 1 - \frac{r+1}{rc_f^2+1}\left(\frac{\omega}{k}\right)^2,$$
$$\left(\frac{\gamma_2}{k}\right)^2 = 1 - \frac{rc_f^4+1}{c_f^2\left(rc_f^2+1\right)}\left(\frac{\omega}{k}\right)^2 - \frac{i\pi}{\omega}\frac{rc_f^2+1}{rc_f^2}\left(\frac{\omega}{k}\right)^2, \tag{36}$$

and for the coefficients of amplitudes

$$\delta_f = 1 - \frac{\omega r}{i\pi}\frac{1-c_f^2}{1+rc_f^2}, \qquad \delta_s = -rc_f^2\left(1 - \frac{\omega r}{i\pi}\frac{1-c_f^2}{1+rc_f^2}\right). \tag{37}$$

These coefficients of amplitudes for low frequencies are complex while we have seen that those of the high frequency limit are real. This means that here vibrations in z-direction appear. We show schematically the behavior of the amplitudes in the neighbouring figure. The dashed lines show the decreasing of the amplitude for real coefficients of amplitudes, the solid line shows it for complex coefficients where vibrations appear.

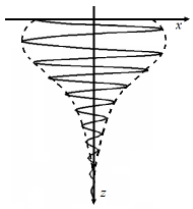

Fig. 4: Behavior of amplitudes of surface waves.
Dashed: real coefficients of amplitudes, solid: complex coefficients of amplitudes.

If we account for the relations (36) and (37) in the condition $\det \mathbf{A} = 0$ then we obtain a relation specifying $\frac{\omega}{k}$. From this we get as a solution a Rayleigh wave whose speed is given by a relation analogous to (35) in which the speeds of bulk waves (7) are replaced by their low frequency counterparts c_{oP1} and c_{oS}:

$$\left(2 - \frac{c_{P1}^2}{c_{oS}^2}\left(\frac{\omega}{k}\right)^2\right)^2 - 4\sqrt{1 - \frac{c_{P1}^2}{c_{oS}^2}\left(\frac{\omega}{k}\right)^2}\sqrt{1 - \frac{c_{P1}^2}{c_{oP1}^2}\left(\frac{\omega}{k}\right)^2} = 0, \tag{38}$$

$$c_{oP1} := \sqrt{\frac{\lambda^S + 2\mu^S + \rho_0^F\kappa}{\rho_0^S + \rho_0^F}}, \qquad c_{oS} := \sqrt{\frac{\mu^S}{\rho_0^S + \rho_0^F}}.$$

Both components move in a synchronized way, thus the influence of diffusion is not visible. This shows that it is often sufficient to use one-component models for the analysis of surface waves in the low frequency range which is the proper region in geophysics.

In contrast to the high frequency approximation this wave is neither dispersive nor dissipative (no attenuation). The Stoneley wave does not exist in this approximation which means, as we see further, that its velocity of propagation is zero in the limit $\omega \to 0$.

2.2 Numerical procedure

The problem $\det \mathbf{A} = 0$ has been solved for the complex wave number, k, using the two computing packages MATLAB 5.3 and MAPLE V Release 5.1. The attempt to execute the calculation with the third package, MATHEMATICA 5, failed. In both successful packages, in principle, it is possible to use the existing equation solvers although they need for the calculations with complex variables a very extensive main memory. It has been observed that the package MAPLE calculates solely *one of the solutions* for k for any choice of sign combinations of exponents γ_1, γ_2 and ζ, changing between branches of solution by the variation of exponents without any apparent reason. Sometimes it was the Rayleigh solution which was calculated and sometimes the Stoneley solution. On the other hand, MATLAB revealed *all solutions* independently of a chosen combination of signs of exponents and this required testing any solution in order to find a corresponding combination of signs. Of course, the ascertained values agreed in both packages.

Inspection of the above solutions shows that they contain roots of quantities which are either already complex or may change the sign. As well known, this means that there exist many Riemann surfaces. It has been seen already in the case of classical Rayleigh waves ([33], [40]) that, in order to obtain a true surface wave one has to choose a proper Riemann plane otherwise one obtains leaky surface waves. This is, of course, also visible in the numerical procedure which yields solutions on both Riemann surfaces which are related to the true surface wave as well as to solutions for leaky waves. An additional problem arises due to the fact that complex solutions in the present case follow not only from the choice of the Riemann surface but also from the attenuation through dissipation. Consequently, a numerical analysis has to be done with a particular care.

The duration of the calculation for one value of ω was about 90s on a 1000 MHz machine.

From the complex results for k we are able to determine the normalized velocities of the Rayleigh and Stoneley modes $c'_{Ra} = \dfrac{\omega}{\operatorname{Re} k_1}$, $c'_{St} = \dfrac{\omega}{\operatorname{Re} k_2}$, respectively, and the corresponding normalized attenuations $\operatorname{Im} k_1$ for the Rayleigh wave and $\operatorname{Im} k_2$ for the Stoneley wave.

2.3 Parameters

The results have been obtained for the following numerical data

$$\begin{array}{llll} \beta = 0, & c_{P1} = 2500\ \dfrac{\mathrm{m}}{\mathrm{s}}, & c_{P2} = 1000\ \dfrac{\mathrm{m}}{\mathrm{s}}, & c_S = 1500\ \dfrac{\mathrm{m}}{\mathrm{s}}, \\ \rho_0^S = 2500\ \dfrac{\mathrm{kg}}{\mathrm{m}^3}, & \rho_0^F = 250\ \dfrac{\mathrm{kg}}{\mathrm{m}^3}, & c_f = \dfrac{c_{P2}}{c_{P1}} = 0.4, & c_s = \dfrac{c_S}{c_{P1}} = 0.6, \\ r = \dfrac{\rho_0^F}{\rho_0^S} = 0.1, & \pi = \left\{ \begin{array}{l} 10^7\ \frac{\mathrm{kg}}{\mathrm{m}^3\mathrm{s}} \text{ or} \\ \text{variable} \end{array} \right., & \tau = 10^{-6}\ \mathrm{s}, & \pi' := \dfrac{\pi\tau}{\rho_0^S} = \left\{ \begin{array}{l} 0.004 \text{ or} \\ \text{variable} \end{array} \right. . \end{array} \tag{39}$$

These data correspond approximately to, for instance, either marls or porous and saturated sandstones [12].

2.4 Numerical results

In the whole range of frequencies there exist two surface modes of propagation corresponding to the classical Rayleigh and Stoneley waves.

Results are shown for different values of the bulk permeability coefficient, π. This parameter describes the resistance of the porous medium against the flow of the fluid.

> The classical form of the Darcy law refers to simple seepage experiments and describes the seepage velocity v_{seep} in terms of the pressure gradient
>
> $$v_{seep} = -\frac{K}{\rho g}\frac{dp}{dx},$$
>
> where ρ – mass density of the fluid, g – earth acceleration, and K – hydraulic conductivity. This corresponds to the quasistatic form of the relation $(1)_2$
>
> $$\frac{dp}{dx} + \pi\left(v^F - v^S\right) = 0,$$
>
> if we require the relative and seepage velocities to be identical $v_{seep} = v^F - v^S$. Consequently, the relation between permeability coefficients in these two approaches is as follows
>
> $$\frac{K}{\rho g} \sim \frac{1}{\pi}.$$
>
> For instance, for water saturated sands $K \sim 10^{-2} \div 10^{-3}\ \frac{\mathrm{m}}{\mathrm{s}}$, $\rho \sim 10^3\ \frac{\mathrm{kg}}{\mathrm{m}^3}$ and $g \sim 10\ \frac{\mathrm{m}}{\mathrm{s}^2}$ $\Longrightarrow \pi \sim 10^6 \div 10^7\ \frac{\mathrm{kg}}{\mathrm{m}^3\mathrm{s}}$ (see e.g. Bear [7]). In standard units of permeability this corresponds to app. $1 \div 0.1$ darcy.

Numerical results for velocities and attenuations are partially normalized. Namely values of velocities are divided by the high frequency velocity of the $P1$-wave c_{P1} given by (39) and these of attenuations – by the product $c_{P1}\tau$.

Consequently, according to relations (20) the normalization of the independent variable ω by the same constant τ would lead to identical results for different values of the permeability coefficient π. This selfsimilarity is lost in the figures presented in the paper due to the fact that we do not normalize the frequency ω. It appears in all figures in real physical units (Hz or MHz).

2.4.1 Phase velocities of Rayleigh and Stoneley waves

Fig. 5 shows the velocity of the Rayleigh wave normalized by the $P1$-velocity in dependence on the frequency (see: (20)). The velocity is given for different values of the bulk permeability parameter π. The left and the right figure differ in the range of frequencies. In the left one it varies between zero and the very large value of 100 MHz while the range in the right one is smaller. As in the classical case velocities of all monochromatic Rayleigh waves are smaller than the velocity of the bulk shear wave, c_S, whose normalized value is $c_s \equiv \frac{c_S}{c_{P1}} = 0.6$. The high and low frequency limits which are indicated in the left

figure are different and correspond to different limits of bulk waves. For our data these dimensionless limits are approx. 0.5493 and 0.5237, respectively.

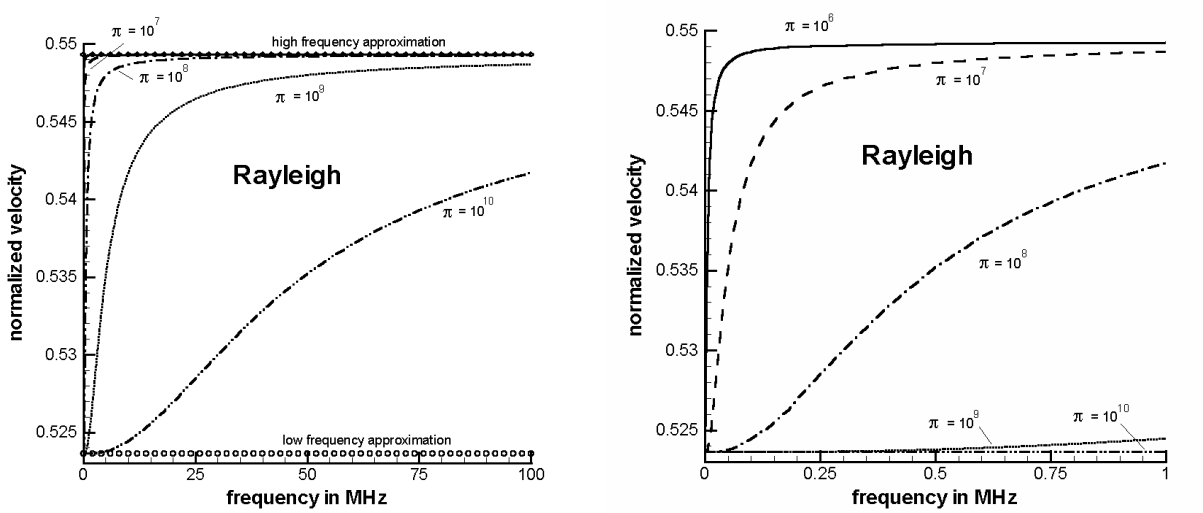

Fig. 5: Normalized velocities of the Rayleigh wave $c'_{Ra} \equiv \frac{c_{Ra}}{c_{P1}}$ for different values of the permeability coefficient π in units $\left[\frac{\mathrm{kg}}{\mathrm{m^3 s}}\right]$ and in different ranges of frequencies.

The velocity of the Rayleigh wave possesses in the range of relatively small frequencies an interesting feature. As we see in the next figure the dependence on the frequency is not monotonous. However, the nonmonotonicity is so weak that in the range of low frequencies applied in geotechnics the Rayleigh velocity may be assumed to be constant. The nonmonotonicity can be observed in a blow-up presented in Fig. 6. The Rayleigh velocity decays first a little and then it becomes growing to its limit value for $\omega \to \infty$. The maximum decay is very little indeed – approx. 0.025% of the difference of limit values for $\omega = 0$ and $\omega \to \infty$. Interestingly, the minimum value remains constant for the different values of π. This means that the decay is not driven by the diffusion. Details are shown in the right figure for the permeability $\pi = 10^7 \frac{\mathrm{kg}}{\mathrm{m^3 s}}$.

Bourbié, Coussy and Zinszner [12] prescribe this effect to an influence of the $P2$-wave, whose velocity goes very rapidly to zero as $\omega \to 0$ and becomes already very small in this range of frequencies. Consequently, it has a bigger influence than in the range of higher frequencies on the behavior of Rayleigh waves. It is interesting that this coupling is present in the simplified model where the coupling term in stresses is absent and bulk modes couple only through boundary conditions. Due to the latter property of the model the size of the effect is very small indeed, even though within the Biot's model it is not very large either (compare: Fig. 6.11 in Bourbié et al. [12], where the maximum corresponds to approx. 0.3%).

In any case this region of the Rayleigh velocity has been investigated particularly carefully to eliminate the possibility of numerical artefacts.

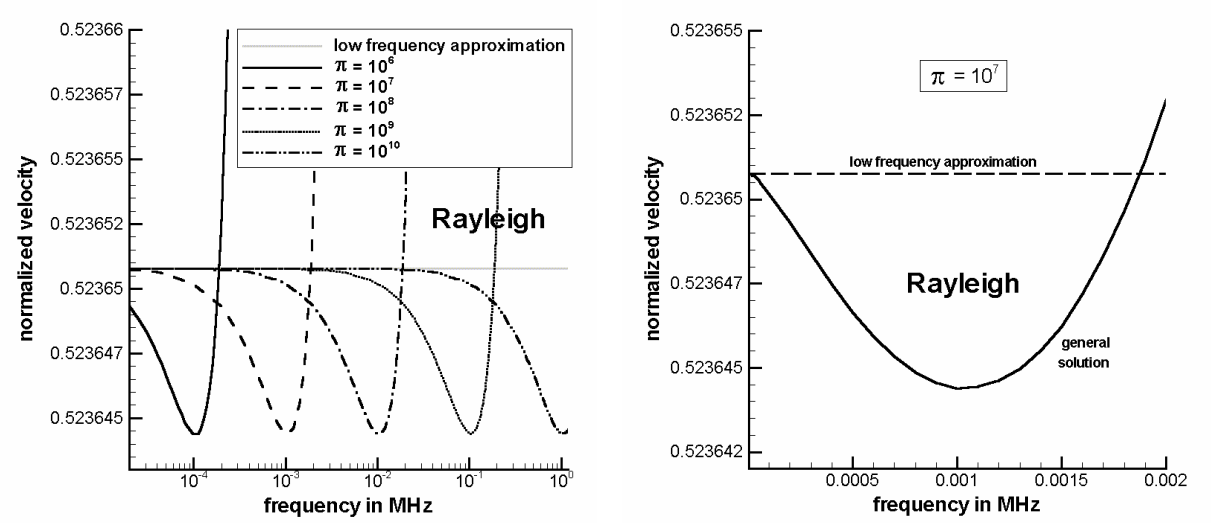

Fig. 6: Decay of the Rayleigh velocity $\frac{c_{Ra}}{c_{P1}}$ in the range of relatively small frequencies. Left: for different values of the permeability coefficient π in units $\left[\frac{\mathrm{kg}}{\mathrm{m^3 s}}\right]$, right: detail for $\pi = 10^7 \frac{\mathrm{kg}}{\mathrm{m^3 s}}$.

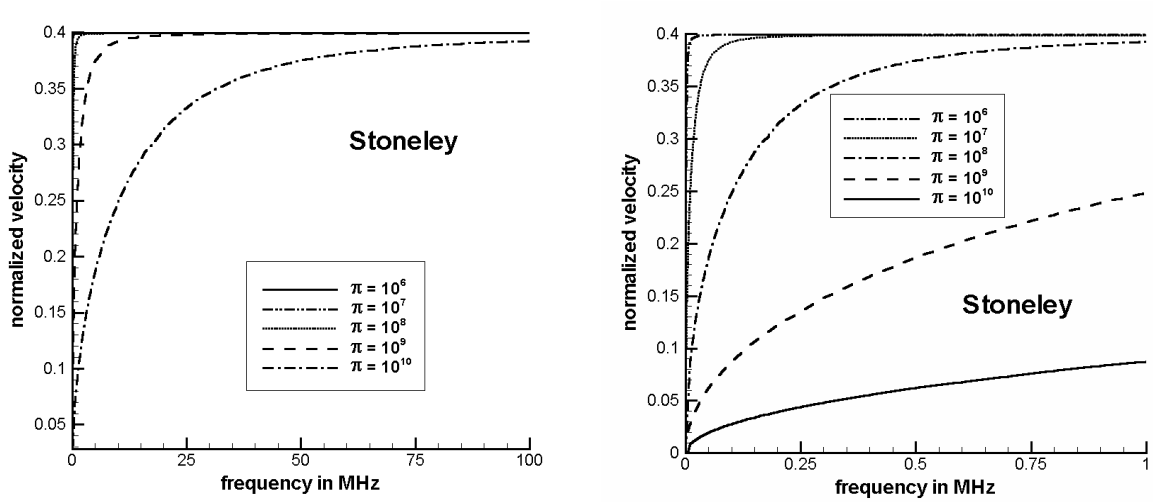

Fig. 7: Normalized velocities of the Stoneley wave $c'_{St} \equiv \frac{c_{St}}{c_{P1}}$ for different values of the permeability coefficient π in units $\left[\frac{\mathrm{kg}}{\mathrm{m^3 s}}\right]$ in different ranges of frequencies.

In Fig. 7 we present the velocity of the second surface wave possible for the boundary porous medium/vacuum – the Stoneley wave. It is normalized in the same way as the Rayleigh velocity. Also in these figures we see the curves for several values of π. The velocity increases from the zero value for $\omega = 0$. This property was indicated earlier as a nonexistence of the Stoneley wave. The growth is faster than the growth of the Rayleigh velocity but the maximum value is smaller. It lies always below the normalized velocity of the fluid $c_f \equiv \frac{c_{P2}}{c_{P1}} = 0.4$. This happens for all values of π. The maximum value of the Stoneley velocity appearing for $\omega \to \infty$ is approximately 0.15% smaller than the velocity of the fluid. One should point out that the Stoneley velocity behaves regularly in the whole range of frequencies and it ceases to exist only for $\omega = 0$. In the vicinity of this

point the Stoneley velocity possesses a similar feature to the $P2$-wave: it decays to zero as $\sqrt{\omega}$.

In order to be more specific, in Fig. 8 we consider a selected case which may appear in geotechnics and shows the normalized velocities of both Rayleigh and Stoneley waves for a permeability coefficient $\pi = 10^7 \frac{\mathrm{kg}}{\mathrm{m^3 s}}$. This corresponds, as shown above, to sandstone saturated with water.

We see the velocities of both surface modes in different ranges of frequencies. The first graph shows properties up to 0.5 MHz, and the second one – up to 10 Hz. Each wave attends a finite asymptotic value as $\omega \to \infty$. This value is bigger for the Rayleigh wave than for the Stoneley wave. While the Stoneley wave velocity starts from zero for $\omega = 0$ the Rayleigh wave yields a low frequency limit unequal to zero. With growing frequency the Rayleigh wave remains at first nearly constant and then increases little until it reaches the high frequency limit. On the other hand the growth of the Stoneley wave velocity is much steeper.

In order to demonstrate the existence of the Stoneley wave in the range of very small frequencies we show in the right figure some calculated points which make obvious that there do not appear any numerical problems to calculate the Stoneley velocity in the limit $\omega \to 0$. In the same range of frequencies, usual in geophysics, the Rayleigh velocity remains nearly constant. Notice that the velocity axis is broken in order to show the behavior of both velocities in the same units.

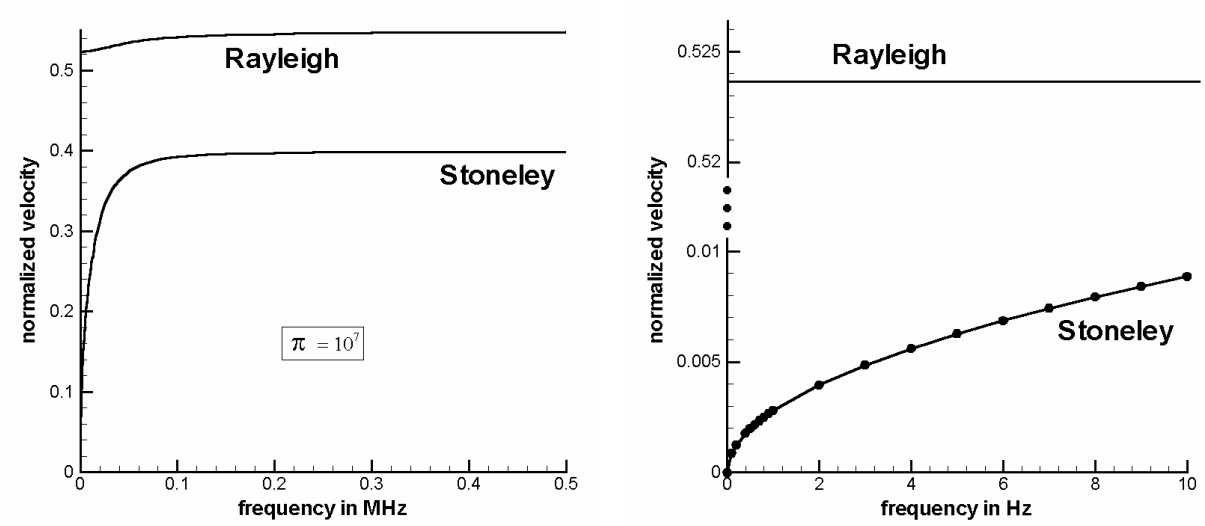

Fig. 8: Comparison of the behavior of Rayleigh and Stoneley wave velocities in high and low frequency ranges for a permeability coefficient $\pi = 10^7 \frac{\mathrm{kg}}{\mathrm{m^3 s}}$.

2.4.2 Group velocities of Rayleigh and Stoneley waves

The figures for phase velocities of Rayleigh and Stoneley waves show that both of them depend on the frequency ω. In inhomogeneous media waves of different frequency (or wavelength) in general propagate with different phase velocities. This phenomenon is known as *dispersion*. The dispersion in heterogeneous materials appears in a nondissipative manner which is not the case in systems with diffusion. It is easy to see that dissipative waves considered in this article become nondispersive in the nondissipative

limit $\pi \to 0$. Compare the chapter of K. Wilmanski in this book [40] where it is shown that in homogeneous media waves propagate undispersed.

A monochromatic wave as investigated in this section is an idealization which is never strictly realized in nature. Most sources emit signals with a continuous spectrum over a limited frequency band. The group velocity c_g (for details in the case of real k see e.g. [1], [9] or[48]) for a given frequency ω is the velocity of transport of a wave package consisting of contributions from a band of frequencies around ω. Then, accounting for the fact that the real wavelength k and the phase velocity c_{ph} depend on the frequency $\left(k = \frac{\omega}{c_{ph}}\right)$

$$\frac{dk}{d\omega} = \frac{1}{c_g} = \frac{1}{c_{ph}} - \frac{\omega}{c_{ph}^2}\frac{dc_{ph}}{d\omega}, \quad \Rightarrow c_g = \frac{c_{ph}}{1 - \frac{\omega}{c_{ph}}\frac{dc_{ph}}{d\omega}}. \tag{40}$$

However, in our case the wave number is complex ($k = k_R(\omega) + ik_I(\omega)$) and a relation similar to (40) follows under some simplifying assumptions. We consider the wave consisting of a narrow band of frequencies near the middle frequency ω_0. The solution for the amplitude A can be described by a Fourier integral which accounts for all frequencies entering the band

$$A(x,t) = \frac{1}{2\pi}\int_{-\infty}^{\infty} A(\omega)\, \mathrm{e}^{-k_I x}\, \mathrm{e}^{i(k_R x - \omega t)}\, d\omega. \tag{41}$$

Under the assumptions of small changes of the amplitude and small changes of damping k_I in the range $\omega_0 \le \omega \le \omega_0 + \Delta\omega$, this is approximately

$$\begin{aligned}
A(x,t) &\cong \frac{1}{2\pi}A(\omega_0)\, \mathrm{e}^{-k_I^0 x}\, \mathrm{e}^{i\left(k_R^0 x - \omega_0 t\right)} \int_{\omega_0}^{\omega_0+\Delta\omega} \mathrm{e}^{i\left(\frac{x}{c_g} - t\right)(\omega - \omega_0)}\, d\omega \cong \\
&\cong \frac{1}{2\pi}A(\omega_0)\, \mathrm{e}^{i(k_0 x - \omega_0 t)} \int_0^{\Delta\omega} \mathrm{e}^{i\left(\frac{x}{c_g} - t\right)\xi}\, d\xi = \\
&= \frac{1}{2\pi}A(\omega_0)\, \mathrm{e}^{i(k_0 x - \omega_0 t)} \int_0^{\Delta\omega} \left[\cos\left(\frac{x}{c_g} - t\right)\xi + i\sin\left(\frac{x}{c_g} - t\right)\xi\right] d\xi = \\
&= \frac{1}{2\pi}A(\omega_0)\, \mathrm{e}^{i(k_0 x - \omega_0 t)}\, \frac{1}{\frac{x}{c_g} - t} \left[\sin\left(\frac{x}{c_g} - t\right)\Delta\omega - i\underbrace{\left(\cos\left(\frac{x}{c_g} - t\right)\Delta\omega - 1\right)}_{\approx 0}\right] = \\
&= \frac{1}{2\pi}A(\omega_0)\, \underbrace{\mathrm{e}^{ik_0\left(x - c_{ph}t\right)}}_{\text{carrier}} \underbrace{\left(\frac{\sin\left[\left(\frac{x}{c_g} - t\right)\Delta\omega\right]}{\left(\frac{x}{c_g} - t\right)\Delta\omega}\right)}_{\text{modulator}} \Delta\omega,
\end{aligned} \tag{42}$$

$$\text{with} \quad \boxed{c_g := \left(\frac{dk_R}{d\omega}\right)^{-1}_{\omega=\omega_0} = \frac{c_{ph}}{1 - \frac{\omega}{c_{ph}}\frac{dc_{ph}}{d\omega}}} \quad \text{and} \quad \left|\frac{\Delta\omega}{\omega_0}\right| \ll 1, \quad c_{ph} = \frac{\omega}{k_R}$$

$$k_0 = k_R^0 + ik_I^0 = k(\omega_0).$$

In the following figure we show both the phase velocities and the group velocities of both surface waves at the boundary porous medium/vacuum for the permeability coefficient $\pi = 10^7\ \frac{\mathrm{kg}}{\mathrm{m^3 s}}$. The derivative $\frac{dc_{ph}}{d\omega}$ has been calculated as central difference.

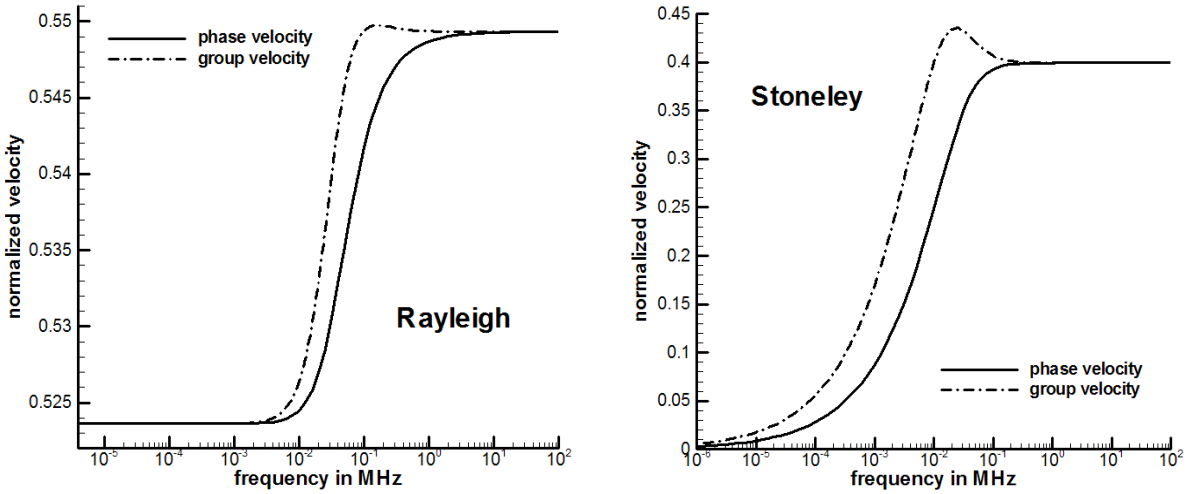

Fig. 9: Rayleigh and Stoneley wave phase and group velocities in the whole frequency range for a permeability coefficient $\pi = 10^7 \frac{\mathrm{kg}}{\mathrm{m^3 s}}$.

We see that both group velocities have a maximum while these maxima do not appear in the phase velocity curves. Consequently, even though we have the inverse behavior to this typical for classical elastic systems (phase speeds grow rather than decay with the frequency ω), we may expect sharp changes in the amplitude of arriving waves. These correspond to the classical Airy phase, namely amplitudes at the time in a seismogram at which sharp pulses arrive (see chapter of Wilmanski [40]).

2.4.3 Attenuation of Rayleigh and Stoneley waves

This section is devoted to the behavior of the attenuation of the Rayleigh and Stoneley waves. Imaginary parts of the wave number k determine the damping of waves. It is normalized by the product with the $P1$-velocity and the relaxation time (see: (20)). This means for our parameters that the values presented in the figures are 400 times smaller $((2500 \times 10^{-6})^{-1})$ than in real physical units $\left[\frac{1}{\mathrm{m}}\right]$.

Let us first turn our attention to the Rayleigh wave. Fig. 10 shows the attenuation of this wave in different ranges of frequency. The left hand side conveys the impression that the attenuation would not start from zero with zero frequency. This stems from the double-logarithmic scale. However, in the right figure (at least at the frequency-axis) the right physical behavior is obvious: the attenuation for all values of π starts from zero. Although distorting the $\omega - \mathrm{Im}\, k$ behavior, we use on the left hand side the double-logarithmic scale to expose two characteristic features: intersections of curves for different permeabilities π as well as the common asymptotics for $\omega \to \infty$. In contrast to all other waves whose attenuation goes to a finite limit as $\omega \to \infty$ – a property which, incidentally, was not clearly stated in earlier works – the attenuation of Rayleigh waves goes to ∞ as $\omega \to \infty$. We demonstrate this point separately again in Fig. 13 but we want to stress here that this singular behavior of the Rayleigh wave in relation to the attenuation is the feature of a *leaky wave*. In contrast to the attenuation of other waves which results solely from the dissipation, for a leaky wave the infinite limit of attenuation (asymptote) is independent of the permeability π, provided $\pi \neq 0$. The left hand side of

Fig. 10 also clarifies that the attenuation is in the same manner selfsimilar as the velocity. The existence of intersection points of curves for different π is also characteristic for bulk $P1$-waves and indicates the decay of curvature of these curves as functions of the physical frequency ω with the growing permeability π.

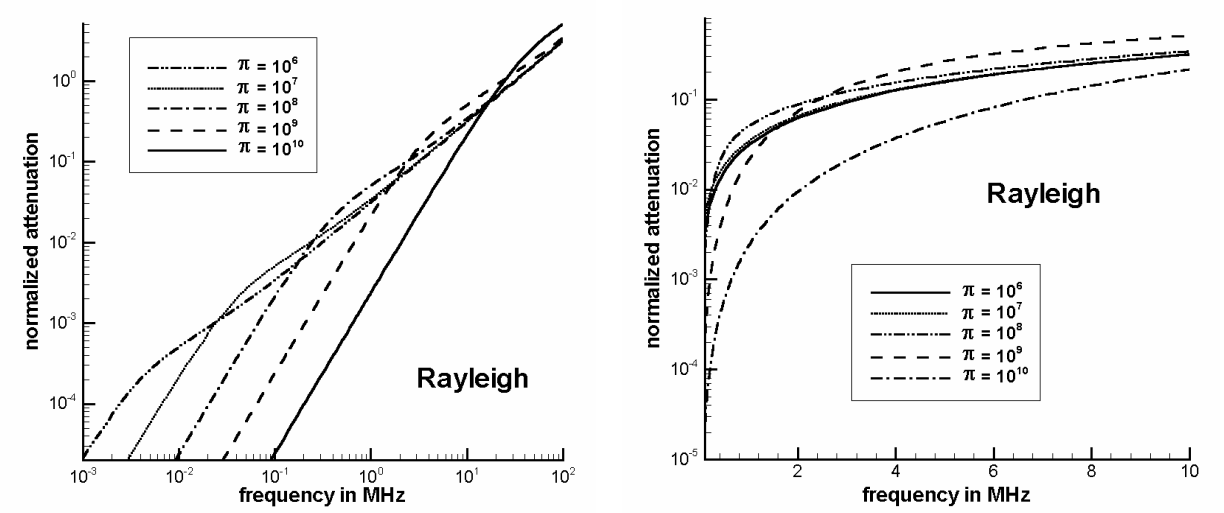

Fig. 10: Attenuation of the Rayleigh wave for different values of the permeability coefficient π in units $\left[\frac{\mathrm{kg}}{\mathrm{m^3 s}}\right]$ in different ranges of frequencies.

In order to expose a region of very small frequencies important in geotechnical applications, we present in Fig. 11 the attenuation of both surface waves and two bulk waves: $P1$ and $P2$ in the range of frequencies up to 1000 Hz. Clearly, in this range, the Rayleigh wave is attenuated stronger than the $P1$ wave but still weaker than $P2$.

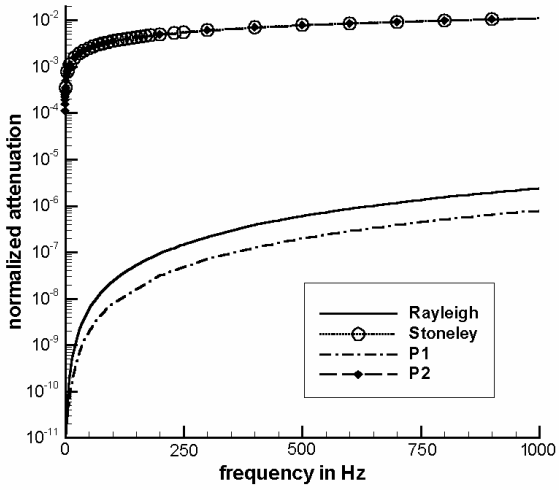

Fig. 11: Attenuation of Rayleigh, Stoneley, $P1$ and $P2$-wave, for $\pi = 10^7 \frac{\mathrm{kg}}{\mathrm{m^3 s}}$ in a range of small frequencies.

Inspection of Fig. 12 shows that also the normalized attenuation of the Stoneley wave starts from the zero value for $\omega = 0$. But, in contrast to the Rayleigh wave attenuation for small frequencies, it increases much faster and then approaches a horizontal asymptotic value for larger values of the frequency. This means that the limit $\omega \to \infty$ is finite and dependent on the permeability coefficient π.

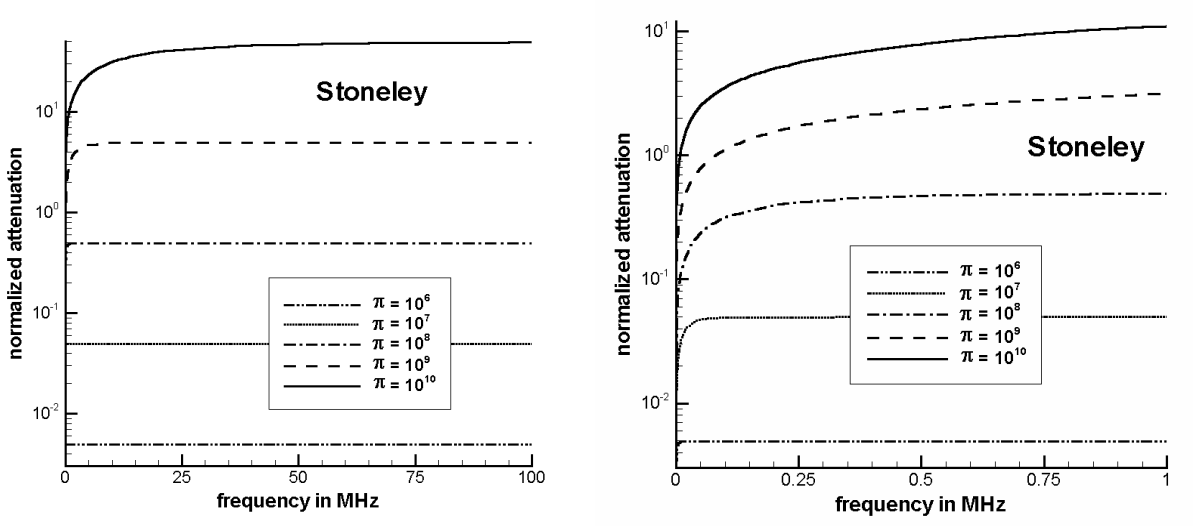

Fig. 12: Attenuation of the Stoneley wave for different values of the permeability coefficient π in units $\left[\frac{\mathrm{kg}}{\mathrm{m^3 s}}\right]$ in different ranges of frequencies.

This property does not coincide with the statement in Edelman, Wilmanski [18] in which it is claimed that the Stoneley wave propagates "almost without attenuation" (p. 38). This feature concerns the quantity $\operatorname{Im}\tilde{\omega} \equiv \frac{\operatorname{Im}\omega}{k}$ in terms of the quoted paper, and means solely that $\lim\limits_{k\to\infty} \operatorname{Im}\omega < \infty$. In the frequency space considered in the present work we have similarly $\lim\limits_{\omega\to\infty} \operatorname{Im} k < \infty$.

We can reinterpret those results in terms of the *quality factor* used frequently in works on acoustics. As indicated, for instance, in Aki and Richards [1], Bourbie et al. [12] it may be defined as

$$Q(\omega) := \left|\frac{\operatorname{Re} k(\omega)}{\operatorname{Im} k(\omega)}\right| \equiv \left|\frac{\operatorname{Re} k(\omega)}{\omega}\frac{\omega}{\operatorname{Im} k(\omega)}\right| = \frac{1}{c_{ph}}\left|\frac{\omega}{\operatorname{Im} k(\omega)}\right|, \quad c_{ph} := \frac{\omega}{\operatorname{Re} k(\omega)}. \tag{43}$$

Clearly, for $|\operatorname{Im} k(\omega)| < \infty$, we have the limit $\lim\limits_{\omega\to\infty} Q(\omega) = \infty$, which is qualified in these works as a lack of dissipation. The other limit $Q = 0$ would mean an infinitely attenuating medium.

We do not use the notion of the quality factor in this article because neither its definition (43) is universally accepted, particularly for the limit $\omega \to 0$, nor it possesses such a clear physical interpretation as $\operatorname{Im} k$.

In Fig. 13 we show the normalized attenuation of the surface and bulk waves. For low frequencies the attenuation of the Stoneley wave is much higher than this of the Rayleigh wave. Both attenuations are starting from zero for $\omega = 0$. The Stoneley wave attenuation increases rapidly until it reaches a certain value which depends on the permeability coefficient π, in the case under consideration – approx. $0.0496\times (c_{P1}\tau)^{-1} \simeq 19.84\frac{1}{\mathrm{m}}$. After reaching this value – which happens in the low frequency range – it remains almost constant. The Rayleigh wave attenuation, however, does not have a finite value for $\omega \to \infty$. As we have already mentioned, the Rayleigh wave is for this reason a leaky wave. Generally, the Rayleigh attenuation increases linearly with growing ω (i.e. the corresponding

quality factor $\lim_{\omega\to\infty} Q(\omega) < \infty$), only for very low frequencies the growth is a little bit faster. Consequently, there appears an intersection of the attenuation curves of both waves. This point lies in the range of high frequencies.

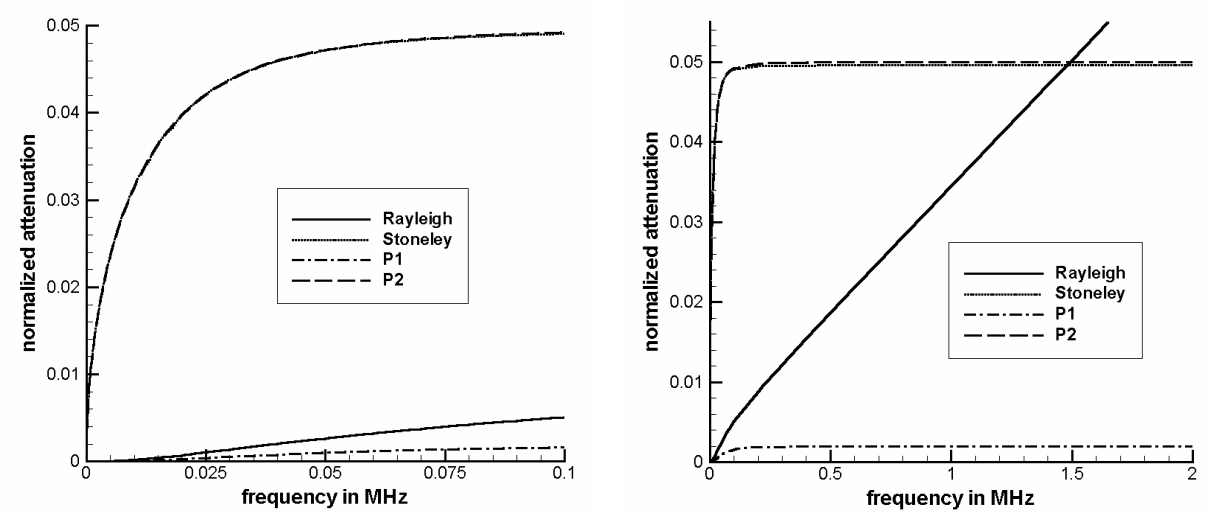

Fig. 13: Normalized attenuation of Rayleigh, Stoneley, $P1$ and $P2$-wave, for $\pi = 10^7\ \frac{\mathrm{kg}}{\mathrm{m^3 s}}$ in different ranges of frequencies.

2.5 Summary of results for boundary porous medium/vacuum

In the whole range of frequencies there exist two modes of surface waves: a leaky Rayleigh wave and a Stoneley wave. We have shown numerical results for the normalized velocities $\left(\frac{1}{c_{P1}}\frac{\omega}{\operatorname{Re} k(\omega)}\right)$ and attenuations $(\operatorname{Im} k(\omega)\, c_{P1}\tau)$ of these waves for different values of the bulk permeability coefficient, π, in different ranges of frequencies, ω.

Leaky Rayleigh

- the velocity of propagation of this wave lies in the interval determined by the limits $\omega \to 0$ (following from (38)) and $\omega \to \infty$ (following from (34)). The high frequency limit is approx. 4.7% higher than the low frequency limit. The velocity is always smaller than c_S, i.e. slower than the S-wave. As a function of ω it possesses an inflection point and it is slightly nonmonotonous,

- this nonmonotonicity appears in the range of small frequencies. The velocity possesses in this range a minimum whose size is very small (approx. 0.025% of the difference of limit values for $\omega = 0$ and $\omega \to \infty$). Interestingly, the minimum value remains constant for the different values of π. This means that the decay is not driven by diffusion. Such a behavior is also observed within Biot's model. It results from a coupling of $P1$- and $P2$-waves through boundary conditions;

- the attenuation of this wave grows from zero for $\omega = 0$ to infinity as $\omega \to \infty$. In the range of large frequencies it is linear (i.e. the quality factor is a constant different from zero) and independent of the permeability π. This means that it is a leaky wave.

Stoneley

- the velocity of this wave grows monotonically from the zero value for $\omega = 0$ to a finite limit which is slightly smaller (approx. 0.15%) than the velocity c_{P2} of the $P2$-wave. The growth of the velocity of this wave in the range of low frequencies is much steeper than this of Rayleigh waves similarly to the growth of the $P2$-velocity;
- both the velocity and attenuation of the Stoneley wave approach zero as $\sqrt{\omega}$,
- the attenuation of the Stoneley wave grows monotonically to a finite limit for $\omega \to \infty$. It is slightly smaller than the attenuation of $P2$-waves. Consequently, in contrast to the claims in the literature, the Stoneley wave is attenuated. Solely its quality factor goes to zero as $\omega \to \infty$.

Results for different values of the permeability coefficient π are selfsimilar, i.e. a change of π yields a corresponding change in the scale of the frequency axis for velocities, and of both axes for attenuations. Otherwise the qualitative behavior remains unchanged.

3 Analysis by means of the "simple mixture model" – boundary porous medium/fluid

In the previous part we have introduced the equations for the porous medium. Investigating the interface between a porous medium and a liquid we have to consider additional equations for the liquid outside of the porous medium. We distinguish this part of the system by the sign "+".

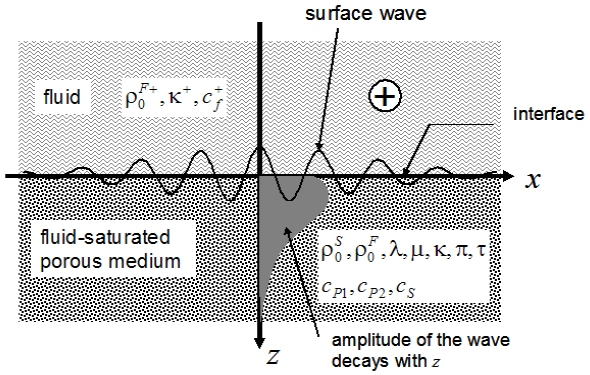

Fig. 14: Geometry of the interface porous medium/fluid.

3.1 Construction of solution

The additional equations for the fluid in the exterior of the porous material read

$$\begin{aligned} &\frac{\partial \rho^{F+}}{\partial t} + \rho_0^{F+} \operatorname{div} \mathbf{v}^{F+} = 0, \\ &\rho_0^{F+} \frac{\partial \mathbf{v}^{F+}}{\partial t} + \kappa^+ \operatorname{grad} \rho^{F+} = 0. \end{aligned} \tag{44}$$

Here ρ^{F+} denotes the partial mass density of the fluid in the +-region and ρ_0^{F+} is its constant reference value. κ^+ describes the compressibility of the fluid. The identification

of compressibility coefficients in porous materials can be done in many ways and they do not necessarily give the same results. To make this issue clear, we present here two approaches.

One of them is commonly used in micro-macro transitions for granular materials. Such a transition is described by relations $\rho^F = n\rho^{F+}$, $p^F = np^{F+}$, $p^F - p_0^F = \kappa\left(\rho^F - \rho_0^F\right)$, $p^{F+} - p_0^{F+} = \kappa^+\left(\rho^{F+} - \rho_0^{F+}\right)$, and, under the condition of constant porosity $n = n_0$, we have $\kappa = \kappa^+$.

However, a simple wave analysis shows that this relation cannot hold as the speeds of waves carried by the fluid component are, respectively, $c_+ = \sqrt{\kappa^+}$, $c_{P2} = \sqrt{\kappa}$, and these are, of course, different. The situation does not improve essentially if we introduce the Biot's coupling. This means that linear models used in the description of waves cannot be based on the above quoted simple micro-macro relations. They possess their own macroscopic status and their effective material parameters account for such microscopic effects as scattering of waves. Different macroscopic compressibilities for the same material inside and outside of the porous medium are caused by the channels of the porous medium. While a wave can take a free "path" in the fluid outside, inside the porous medium waves are slower due to reflection on the boundaries of the channels. This is, certainly, not present in simple micro-macro transitions.

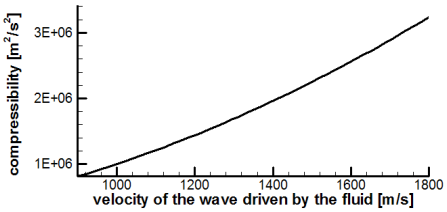

Fig. 15: Compressibilities for different fluid velocities

We assume the fluid to be water. A wave in water travels with the velocity of around $c_+ \approx 1500\ \frac{\mathrm{m}}{\mathrm{s}}$ and the corresponding compressibility $\kappa^+ = 2.25 \cdot 10^6\ \frac{\mathrm{m}^2}{\mathrm{s}^2}$. Inside the porous medium the velocity of the $P2$-wave is assumed to be $c_{P2} = 1000\ \frac{\mathrm{m}}{\mathrm{s}}$ to which corresponds a compressibility $\kappa = c_{P2}^2 = 1 \cdot 10^6\ \frac{\mathrm{m}^2}{\mathrm{s}^2}$ (see Fig.15).

3.1.1 Compatibility with field equations

As also done in the equations for the porous medium we introduce the displacement vector $\mathbf{u}^{F+}$. But it also is introduced solely for technical symmetry of the considerations and it does not have any physical bearing. Then

$$\mathbf{u}^{F+} = \operatorname{grad}\varphi^{F+}, \quad \mathbf{v}^{F+} = \frac{\partial \mathbf{u}^{F+}}{\partial t}. \tag{45}$$

Again, we make an ansatz for solutions harmonic in the x-direction

$$\begin{aligned} \varphi^{F+} &= A^{F+}(z)\exp\left[i\left(kx - \omega t\right)\right], \\ \rho^{F+} - \rho_0^{F+} &= A_\rho^{F+}(z)\exp\left[i\left(kx - \omega t\right)\right]. \end{aligned} \tag{46}$$

Substitution in (44) leads to the following compatibility conditions

$$A_\rho^{F+} = -\rho_0^{F+}\left(\frac{d^2}{dz^2} - k^2\right)A^{F+}, \qquad \left[\kappa^+\left(\frac{d^2}{dz^2} - k^2\right) + \omega^2\right]A^{F+} = 0. \tag{47}$$

We introduce dimensionless quantities

$$c_f^+ := \frac{\sqrt{\kappa^+}}{c_{P1}}, \quad r^+ := \frac{\rho_0^{F+}}{\rho_0^S} < 1, \quad \alpha' := \alpha c_{P1}. \tag{48}$$

Further we omit the prime. Then substitution of (20) and (48) in equations (47) yields

$$\left[c_f^{+2}\left(\frac{d^2}{dz^2} - k^2\right) + \omega^2\right] A^{F+} = 0. \tag{49}$$

We seek a solution in the form

$$A^{F+} = A_f^+ e^{\gamma^+ z}, \tag{50}$$

where the exponent γ^+ must possess a positive real part to describe a surface wave. Substitution in (49) yields it in the form

$$\left(\frac{\gamma^+}{k}\right)^2 = 1 - \frac{1}{c_f^{+2}}\left(\frac{\omega}{k}\right)^2 \quad \Rightarrow \quad \boxed{\frac{\gamma_{1,2}^+}{k} = \pm\sqrt{1 - \frac{1}{c_f^{+2}}\left(\frac{\omega}{k}\right)^2}.} \tag{51}$$

3.1.2 Insertion into boundary conditions

Using (11) and (45) we get (not yet dimensionless)

$$\begin{aligned}
&\bullet \quad \left(2\frac{\partial^2\varphi^S}{\partial x\partial z} + \frac{\partial^2\psi_y^S}{\partial x^2} - \frac{\partial^2\psi_y^S}{\partial z^2}\right)\Big|_{z=0} = 0, \\
&\bullet \quad c_{P1}^2\rho_0^S\left(\frac{\partial^2\varphi^S}{\partial x^2} + \frac{\partial^2\varphi^S}{\partial z^2}\right) - 2c_S^2\rho_0^S\left(\frac{\partial^2\varphi^S}{\partial x^2} - \frac{\partial^2\psi_y^S}{\partial x\partial z}\right) + \\
&\qquad + c_+^2\left(\rho^{F+} - \rho_0^{F+}\right) - c_{P2}^2\left(\rho^F - \rho_0^F\right)\big|_{z=0} = 0, \\
&\bullet \quad \rho_0^F\frac{\partial}{\partial t}\left(\frac{\partial\varphi^F}{\partial z} + \frac{\partial\psi_y^F}{\partial x} - \frac{\partial\varphi^S}{\partial z} - \frac{\partial\psi_y^S}{\partial x}\right)\Big|_{z=0} = \rho_0^{F+}\frac{\partial}{\partial t}\left(\frac{\partial\varphi^{F+}}{\partial z} - \frac{\partial\varphi^S}{\partial z} - \frac{\partial\psi_y^S}{\partial x}\right)\Big|_{z=0}, \\
&\bullet \quad \rho_0^F\frac{\partial}{\partial t}\left(\frac{\partial\varphi^F}{\partial z} + \frac{\partial\psi_y^F}{\partial x} - \frac{\partial\varphi^S}{\partial z} - \frac{\partial\psi_y^S}{\partial x}\right)\Big|_{z=0} + \alpha\left\{p_0^F + c_{P2}^2\left(\rho^F - \rho_0^F\right) - \right. \\
&\qquad \left. - n_0\left[p_0^{F+} + c_+^2\left(\rho^{F+} - \rho_0^{F+}\right)\right]\right\}\big|_{z=0} = 0,
\end{aligned} \tag{52}$$

where we have used the constitutive relations

$$\begin{gathered}
p^F = p_0^F + \kappa\left(\rho^F - \rho_0^F\right), \quad p^{F+} = p_0^{F+} + \kappa^+\left(\rho^{F+} - \rho_0^{F+}\right), \\
c_{P2}^2 = \kappa, \quad c_+^2 = \kappa^+.
\end{gathered} \tag{53}$$

Making use of (13), (14), (16), (46) and (47) we obtain

$$\bullet \quad \left(-k^2B^S - \frac{d^2B^S}{dz^2} + 2ik\frac{dA^S}{\partial z}\right)\Big|_{z=0} = 0, \tag{54}$$

- $c_{P1}^2\rho_0^S\left(-k^2A^S+\dfrac{d^2A^S}{dz^2}\right)-2c_S^2\rho_0^S\left(-k^2A^S-ik\dfrac{dB^S}{dz}\right)+$
$+c_{P2}^2\rho_0^F\left(\dfrac{d^2A^F}{dz^2}-k^2A^F\right)-c_+^2\rho_0^{F+}\left(\dfrac{d^2A^{F+}}{dz^2}-k^2A^{F+}\right)\Big|_{z=0}=0,$
- $-i\omega\rho_0^F\left(\dfrac{dA^F}{\partial z}+ikB^F-\dfrac{dA^S}{\partial z}-ikB^S\right)\Big|_{z=0}=$ $(54)_{\text{cont.}}$
$=-i\omega\rho_0^{F+}\left(\dfrac{dA^{F+}}{\partial z}-\dfrac{dA^S}{\partial z}-ikB^S\right)\Big|_{z=0},$
- $i\omega\rho_0^F\left(\dfrac{dA^F}{\partial z}+ikB^F-\dfrac{dA^S}{\partial z}-ikB^S\right)\Big|_{z=0}=\alpha\left\{-c_{P2}^2\rho_0^F\left(\dfrac{d^2A^F}{dz^2}-k^2A^F\right)+\right.$
$\left.+n_0c_+^2\rho_0^{F+}\left(\dfrac{d^2A^{F+}}{dz^2}-k^2A^{F+}\right)\right\},$

where it was assumed that

$$p_0^{F+}=\frac{p_0^F}{n_0}. \tag{55}$$

It means that the initial external pressure is equal to the initial pore pressure.

Eqs. (54) read in dimensionless form (again omitting the primes)

- $\left(-k^2B^S-\dfrac{d^2B^S}{dz^2}+2ik\dfrac{dA^S}{\partial z}\right)\Big|_{z=0}=0,$
- $-k^2A^S+\dfrac{d^2A^S}{dz^2}+2c_s^2\left(k^2A^S+ik\dfrac{dB^S}{dz}\right)+$ (56)
$+c_f^2r\left(\dfrac{d^2A^F}{dz^2}-k^2A^F\right)-c_f^{+2}r^+\left(\dfrac{d^2A^{F+}}{dz^2}-k^2A^{F+}\right)\Big|_{z=0}=0,$
- $r\left(\dfrac{dA^F}{\partial z}+ikB^F-\dfrac{dA^S}{\partial z}-ikB^S\right)\Big|_{z=0}=r^+\left(\dfrac{dA^{F+}}{\partial z}-\dfrac{dA^S}{\partial z}-ikB^S\right)\Big|_{z=0},$
- $-i\omega\left(\dfrac{dA^F}{\partial z}+ikB^F-\dfrac{dA^S}{\partial z}-ikB^S\right)\Big|_{z=0}=\alpha\left\{c_f^2\left(\dfrac{d^2A^F}{dz^2}-k^2A^F\right)-\right.$
$\left.-\underbrace{n_0\dfrac{r^+}{r}}_{=1}c_f^{+2}\left(\dfrac{d^2A^{F+}}{dz^2}-k^2A^{F+}\right)\right\}.$

where we have used the relation $n_0=\frac{r}{r^+}$ if $r^+\neq 0$.

3.1.3 Dispersion relation

Inserting (16), (22) and (50) in these boundary conditions we obtain

- $-k^2B_s-\zeta^2B_s+2ik\left(\gamma_1A_s^1+\gamma_2A_s^2\right)=0,$ (57)
- $-k^2\left(A_s^1+A_s^2\right)+\gamma_1^2A_s^1+\gamma_2^2A_s^2+2c_s^2\left[k^2\left(A_s^1+A_s^2\right)+ik\zeta B_s\right]+$
$+c_f^2r\left(\gamma_1^2A_f^1+\gamma_2^2A_f^2-k^2A_f^1-k^2A_f^2\right)-c_f^{+2}r^+\left(\gamma^{+2}A_f^+-k^2A_f^+\right)=0,$
- $\gamma_1A_f^1+\gamma_2A_f^2-\dfrac{k\pi}{r\omega+i\pi}B_s+\left(\dfrac{r^+}{r}-1\right)\left(\gamma_1A_s^1+\gamma_2A_s^2+ikB_s\right)-\dfrac{r^+}{r}\gamma^+A_f^+=0,$

$$\bullet \quad -i\omega\left(\gamma_1 A_f^1+\gamma_2 A_f^2-\frac{k\pi}{r\omega+i\pi}B_s-\gamma_1 A_s^1-\gamma_2 A_s^2-ikB_s\right)= \qquad (57)_{\text{cont.}}$$
$$\alpha\left\{c_f^2\left(\gamma_1^2 A_f^1+\gamma_2^2 A_f^2-k^2 A_f^1-k^2 A_f^2\right)-c_f^{+2}\left(\gamma^{+2}A_f^+-k^2 A_f^+\right)\right\}.$$

Now (27) yields the following equations for the four unknown constants B_s, A_s^1, A_f^2, A_f^+

$$\mathbf{AX}=\mathbf{0}, \tag{58}$$

where

$$\mathbf{A} \;:=\; \begin{pmatrix} \left(\frac{\zeta}{k}\right)^2+1 & -2i\frac{\gamma_1}{k} \\ 2ic_s^2\frac{\zeta}{k} & \left(\frac{\gamma_1}{k}\right)^2-1+2c_s^2+ \\ & +rc_f^2\left[\left(\frac{\gamma_1}{k}\right)^2-1\right]\delta_f \\ -\frac{\pi}{r\omega+i\pi}+i\left(\frac{r^+}{r}-1\right) & \frac{\gamma_1}{k}\left[\delta_f+\left(\frac{r^+}{r}-1\right)\right] \\ \frac{r\omega}{r\omega+i\pi}\frac{\omega}{k} & i\frac{\omega}{k}\frac{\gamma_1}{k}\left(\delta_f-1\right)+ \\ & +\alpha c_f^2\left[\left(\frac{\gamma_1}{k}\right)^2-1\right]\delta_f \end{pmatrix} \tag{59}$$

$$\begin{pmatrix} -2i\frac{\gamma_2}{k}\delta_s & 0 \\ \left[\left(\frac{\gamma_2}{k}\right)^2-1+2c_s^2\right]\delta_s+ & -r^+c_f^{+2}\left[\left(\frac{\gamma^+}{k}\right)^2-1\right] \\ +rc_f^2\left[\left(\frac{\gamma_2}{k}\right)^2-1\right] & \\ \frac{\gamma_2}{k}\left[1+\delta_s\left(\frac{r^+}{r}-1\right)\right] & -\frac{r^+}{r}\frac{\gamma^+}{k} \\ i\frac{\omega}{k}\frac{\gamma_2}{k}\left(1-\delta_s\right)+ & \\ +\alpha c_f^2\left[\left(\frac{\gamma_2}{k}\right)^2-1\right] & -\alpha c_f^{+2}\left[\left(\frac{\gamma_+}{k}\right)^2-1\right] \end{pmatrix}, \tag{60}$$

$$\mathbf{X}:=\left(\;B_s,\quad A_s^1,\quad A_f^2,\quad A_f^+\;\right)^T. \tag{61}$$

This homogeneous set yields the *dispersion relation:* $\det\mathbf{A}=0$ determining the $\omega-k$ relation. We investigate also here the solutions of this equation for high and low frequencies.

3.1.4 High and low frequency approximations

High frequencies In the case of high frequencies (physical dimensions) $\frac{1}{\omega\tau}\ll 1$ we have $\delta_s=\delta_f=0$, the exponents $\left(\frac{\gamma_1}{k}\right)^2=1-\left(\frac{\omega}{k}\right)^2$, $\left(\frac{\gamma_2}{k}\right)^2=1-\frac{1}{c_f^2}\left(\frac{\omega}{k}\right)^2$, $\left(\frac{\zeta}{k}\right)^2=1-\frac{1}{c_s^2}\left(\frac{\omega}{k}\right)^2$ and $\left(\frac{\gamma^+}{k}\right)^2=1-\frac{1}{c_f^{+2}}\left(\frac{\omega}{k}\right)^2$, and the dispersion relation follows in the form

$$\alpha \frac{r}{c_s^4} \frac{r}{r^+} \left(\frac{r^+}{r} - 1 \right)^2 \frac{\gamma_1}{k} \left(\frac{\omega}{k} \right)^5 + i \frac{r}{c_s^4} \left(\frac{\gamma^+}{k} - \frac{r^+}{r} \frac{\gamma_2}{k} \right) \frac{\gamma_1}{k} \left(\frac{\omega}{k} \right)^4 + \tag{62}$$
$$+ \alpha \mathcal{P}_R \left(\frac{r}{r^+} \frac{\gamma_2}{k} - \frac{\gamma^+}{k} \right) \frac{\omega}{k} + i \frac{\gamma_2}{k} \frac{\gamma_+}{k} \mathcal{P}_R = 0,$$

where

$$\mathcal{P}_R := \left[2 - \frac{1}{c_s^2} \left(\frac{\omega}{k} \right)^2 \right]^2 - 4 \frac{\gamma_1}{k} \frac{\zeta}{k}. \tag{63}$$

We consider two cases of the dispersion relation (62):

1. $\underline{\alpha = 0}$ (impermeable boundary; i.e. sealed porous medium in contact with an external fluid)

   We get from (62)
   $$\frac{\gamma_+}{k} \frac{\gamma_2}{k} \mathcal{P}_R + \left(\frac{\gamma^+}{k} - \frac{r^+}{r} \frac{\gamma_2}{k} \right) \frac{r}{c_s^4} \frac{\gamma_1}{k} \left(\frac{\omega}{k} \right)^4 = 0. \tag{64}$$

   The case $\alpha = 0$ does not correspond to the case of the boundary porous medium/vacuum which we have considered in the last section because the fluid outside yields a pressure on the boundary. However, if additional to $\alpha = 0$ also $r^+ = 0$ we have the same conditions and (64) must be identical to the Rayleigh dispersion relation for the boundary porous medium/vacuum (34) derived in the last section (see also: [45])
   $$\mathcal{P}_V = \mathcal{P}_R \frac{\gamma_2}{k} + \frac{r}{c_s^4} \frac{\gamma_1}{k} \left(\frac{\omega}{k} \right)^4 = 0. \tag{65}$$

   This is, indeed, true if we cancel $\frac{\gamma^+}{k}$ on both sides after setting r^+ equal to zero.

2. $\underline{\alpha \to \infty}$
   Here, the other two terms of (62) remain and we obtain after division by α
   $$\mathcal{P}_R \left(\frac{\gamma_2}{k} - \frac{r^+}{r} \frac{\gamma^+}{k} \right) + \left(\frac{r^+}{r} - 1 \right)^2 \frac{r}{c_s^4} \frac{\gamma_1}{k} \left(\frac{\omega}{k} \right)^4 = 0. \tag{66}$$

Both equations (64) and (66) remind equation (65) but they are both modified by the influence of the fluid outside.

Low frequencies In contrast to the impermeable boundary with vacuum analytical calculations in this case become very complicated. Therefore, we investigate this case solely on a numerical example.

3.2 Numerical results

3.2.1 Procedure and parameters

In principle the numerical procedure of solution of the problem $\det \mathbf{A} = 0$ for the complex wave number k is the same as described in Sect. 2.2. However, in this more complicated case MATLAB revealed no result. Thus the results of the programs MAPLE 7 and

MAPLE V Release 5.1 were the sole attainable values. Interestingly, MAPLE for some sign combination of exponents produces two solutions which are close to each other but, for most frequencies, not the same.

In order to expose better some properties, we change the input data for c_S. We need as well additional quantities in the exterior:

$$\begin{array}{llll} c_{P1} = 2500\ \frac{\mathrm{m}}{\mathrm{s}}, & c_{P2} = 1000\ \frac{\mathrm{m}}{\mathrm{s}}, & c_S = 1250\ \frac{\mathrm{m}}{\mathrm{s}}, & c_+ = 1500\ \frac{\mathrm{m}}{\mathrm{s}}, \\ \rho_0^S = 2500\ \frac{\mathrm{kg}}{\mathrm{m}^3}, & \rho_0^F = 250\ \frac{\mathrm{kg}}{\mathrm{m}^3}, & \rho_0^{F+} = 1000\ \frac{\mathrm{kg}}{\mathrm{m}^3}, & r = \frac{\rho_0^F}{\rho_0^S} = 0.1, \\ c_f = \frac{c_{P2}}{c_{P1}} = 0.4, & c_s = \frac{c_S}{c_{P1}} = 0.5, & c_f^+ = \frac{c_+}{c_{P1}} = 0.6, & r^+ = \frac{\rho_0^{F+}}{\rho_0^S} = 0.4. \end{array} \tag{67}$$

While some of the results for the boundary porous medium/vacuum have been shown for the varying bulk permeability parameter, π, this coefficient is constant here, namely $\pi = 10^7\ \frac{\mathrm{kg}}{\mathrm{m}^3\mathrm{s}}$. However, instead of this we show for this boundary the influence of the surface permeability, α. We demonstrate that two surface waves, both of them leaky, exist in the whole range of frequencies for each choice of α. They correspond to the classical Rayleigh wave, and to a Stoneley wave which is produced due to presence of the fluid outside the porous medium, respectively. The latter can be supported by the fact that it appears also for the sealed pore situation if there is a fluid outside. Moreover we obtain a third type of wave which appeared also on the boundary porous medium/vacuum, namely a true Stoneley wave. However, this wave exists only for small values of α.

Numerical results for velocities and attenuations are normalized in the same way as indicated in Sect. 2.4.

3.2.2 Dependence of phase velocities and attenuations on the frequency

Fig. 16 shows both the phase velocities and the attenuations of all three surface waves appearing at the interface between a porous halfspace and a fluid halfspace. On the left hand side the velocities are plotted and figures on the right hand side show the attenuations. Both quantities are given for a wide range of frequencies between 1 Hz and 100 MHz. The different curves correspond to various values of the surface permeability parameter α. As explained above, $\alpha = 0$ means that the surface is completely impermeable while $\alpha = \infty$ corresponds to an open pore situation.

In Fig. 16 both the frequency and the attenuations are shown in logarithmic scale while the velocity is presented in normal scale.

Phase velocities Again, the velocity of the Rayleigh wave lies under the velocity of the bulk shear wave, c_S, whose normalized value here is $c_s \equiv \frac{c_S}{c_{P1}} = 0.5$. Curves for different values of α have each a low and a high frequency limit which is unequal to zero. While for small frequencies the velocity is the same independently of α, the high frequency limit decreases with increasing α. For the open pore situation the difference between high and low frequency limits is approximately one half of the difference for a close boundary. Inbetween there is a steep increase of the Rayleigh velocity. The range of frequencies for this increase is smaller for small values of α (10-100 kHz) than for large values of α (1-500 kHz). Moreover for the latter there appears a small plateau in this zone. This may be an

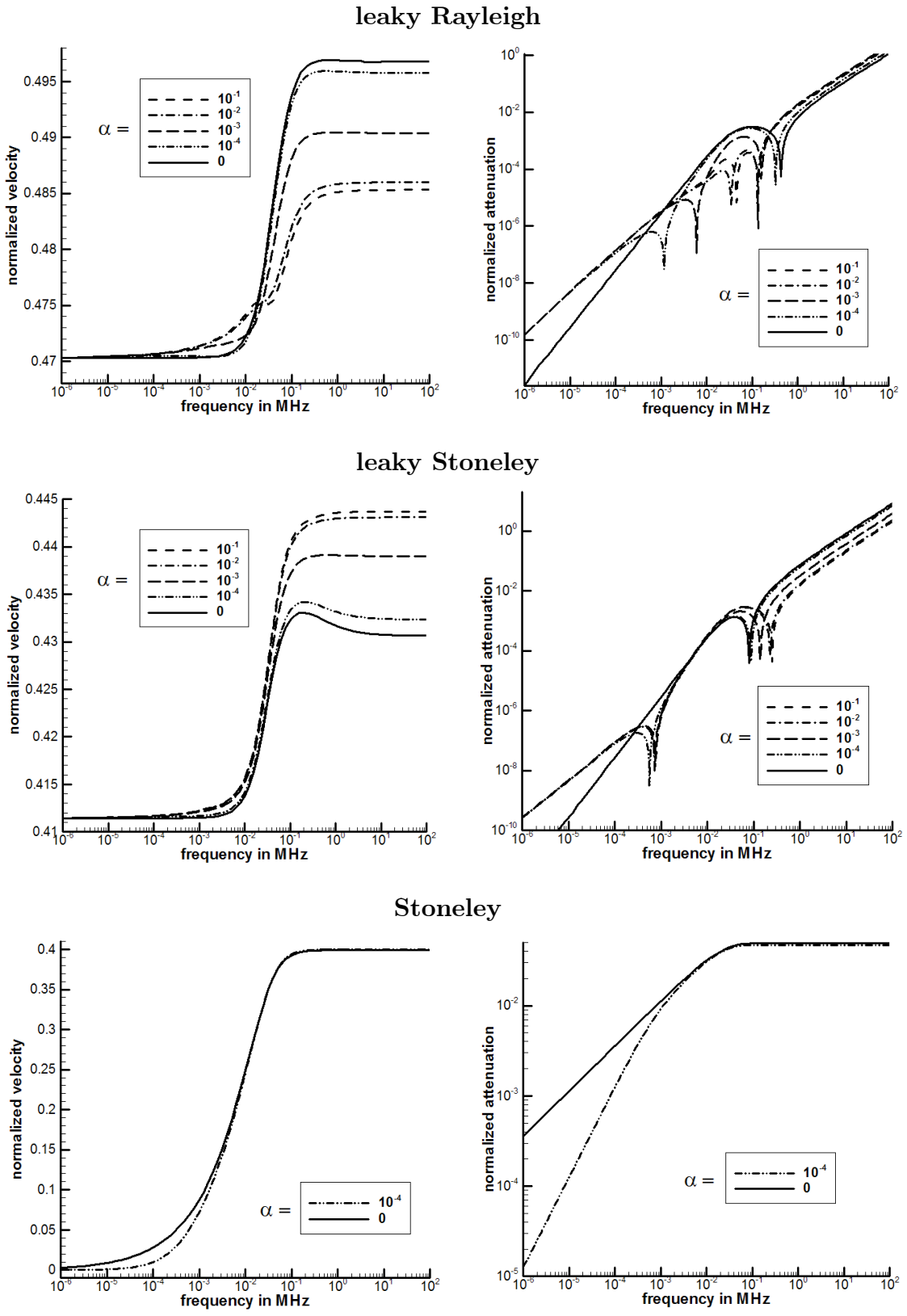

Fig. 16: Normalized phase velocities and attenuations of the leaky Rayleigh, leaky Stoneley and the Stoneley wave in dependence on the frequency. Different curves correspond to different values of the surface permeability α (in units $\left[\frac{\mathrm{s}}{\mathrm{m}}\right]$).
The smaller α the denser the boundary.

indication of the change of the Riemann surface which is, however, much better pronounced in the attenuations.

The velocity of the leaky Stoneley wave behaves similar to the Rayleigh wave. Also this wave possesses high an low frequency limits unequal to zero and the steep increase inbetween appears in the same frequency region. However, in contrast to the Rayleigh wave for this wave the high frequency limit is larger for bigger values of α than for smaller ones. The frequency behavior of this wave is – at least for small α – not monotonous. A maximum value appears in the region of order 100 kHz. Interestingly, the velocity of this wave is smaller than this of the Rayleigh wave although it is driven by the fluid outside of the porous medium whose longitudinal bulk wave is faster than that of the fluid inside the porous medium ($c_f^+ = 0.6$, $c_f = 0.4$). This result has been obtained also by Feng&Johnson [19] within Biot's model. As we will see in the next subsection the true Stoneley wave exists only for small values of α, and, therefore, we show its behavior only for two values of α. For these the velocities do not differ substantially. They start form zero at $\omega = 0$ and increase until around 100 kHz where they reach a high frequency limit which is a little bit smaller than the velocity of the $P2$ wave, $c_f \equiv \frac{c_{P2}}{c_{P1}} = 0.4$.

Attenuations Let us start with the attenuation of the true Stoneley wave. This has the same appearance as this obtained for the boundary porous medium/vacuum. We show a log-log-plot of this attenuation. Thus the similarity to Fig. 12 is not directly obvious. The attenuation starts from zero as $\omega = 0$ and reaches a horizontal asymptote at around 100 kHz. The only amazing point is, that in the mapped region of frequencies, starting from 1 Hz the value for $\alpha = 10^{-4}\ \frac{\mathrm{s}}{\mathrm{m}}$ is much smaller than for $\alpha = 0$ even though the difference in velocities is small. It is surprising because for the other attenuations the value for $\alpha = 0$ lies under all other values for different α.

In contrast to the true surface wave the remaining leaky waves possess singularities in the attenuation for two intermediate frequencies. These frequencies seem to be related with characteristic frequencies $\frac{\pi}{2\rho_0^S}$ and $\frac{\pi}{2\rho_0^F}$ which have already appeared in the stability analysis of adsorption processes [2]. However, there exists an influence of the parameter α, responsible for dissipation, and, simultaneously, the location of the singularities changes with the variation of this coefficient. Consequently, as indicated also in some papers on Biot's model, the diffusion-driven resonances appear also in the surface waves. Their existence seems to be confirmed experimentally (for results of measurements see in particular [13], [47]). On the right we reproduce one figure of the paper [13]. It shows the measured damping coefficients of the pseudo-Stoneley wave (in our terminology: leaky Stoneley wave) in a shock-induced borehole experiment. The formation is a Berea sandstone. The damping coefficient is given in a frequency range up to 50 kHz and we see that there appear also some well pronounced singularities.

Little is known about their mathematical origin. However, the numerical analysis indicates that they appear due to the change of the Riemann surface. If one would ignore the singularities and look only at the connecting line between the maxima the curves would look similar to the curve for the boundary porous medium/vacuum.

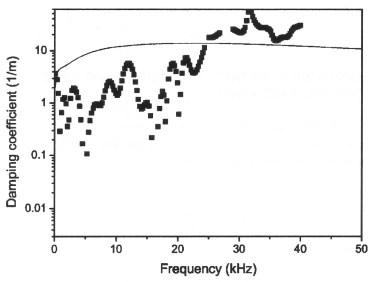

Fig. 17: Experimental damping coefficients of the pseudo-Stoneley wave. From [13].

In any case, it is obvious that the curves show the leaky character as observed already for the Rayleigh wave for this boundary: for high frequencies the attenuation grows linearly and unbounded.

3.2.3 Dependence of phase velocities and attenuations on the surface permeability

In the next figure we illustrate the behavior of the three surface waves appearing at the boundary porous medium/fluid for the frequency limits $\omega \to \infty$, $\omega \to 0$ but in dependence on the surface permeability parameter α. In the first row of Fig. 18 we show normalized velocities and attenuations for the same material parameters as used in the last subsection. In the bottom row the same quantities are shown for another choice of material parameters: with unchanged mass densities and porosity and different velocities for two bulk waves ($c_{P1} = 3500\ \frac{\mathrm{m}}{\mathrm{s}}$, $c_S = 1750\ \frac{\mathrm{m}}{\mathrm{s}}$, c_{P2}, c_{P+} unchanged).

The upper left figure shows the phase velocities of the surface waves for the two limits of frequencies ($\omega \to \infty$ – solid lines, $\omega \to 0$ – dashed lines). Additional to the shown range of surface permeability parameters between $10^{-6}\ \frac{\mathrm{s}}{\mathrm{m}}$ and $10^{-1}\ \frac{\mathrm{s}}{\mathrm{m}}$ we show on the left and right hand side points corresponding to the limit cases $\alpha = 0$ and $\alpha = \infty$. It is obvious that the values for 10^{-6} and 10^{-1} correspond already well to the limit values. While both leaky surface waves exist in the whole range of surface permeabilities, the true surface wave appears only for small values of the surface permeability (approx. in the interval $0 \leq \alpha \leq 10^{-3.9}\ \frac{\mathrm{s}}{\mathrm{m}}$). Thus for a relatively open boundary (large α) no real surface wave exists. It is obvious that for each wave the low frequency value of the velocity (dashed lines) is independent of α. For the true surface wave this value is zero while it is bigger than zero for the leaky waves. Both the high frequency limit of the leaky Rayleigh and of the leaky Stoneley wave change monotonously from the limit $\alpha = 0$ to the limit $\alpha = \infty$. However, the Rayleigh wave velocity is bigger for a dense boundary, while for the leaky Stoneley wave the limit for the open boundary is bigger. The velocity behavior of the waves for the other choice of material parameters ($c_S > c_{f+}$, see: bottom left figure) does not change substantially. Again, $c_R < c_s$, $c_{St} < c_f$ and $c_{leakySt} < c_{f+}$. The latter is a little bit more obvious for this choice of material parameters than for the other choice. We will see in Sect. 4.2 that the last choice corresponds to a higher value of the modulus of the skeleton frame (5.53 instead of 3.95). For this stiffer medium the true Stoneley wave exists only for a still denser boundary, namely for approx. $0 \leq \alpha \leq 10^{-4.8}\ \frac{\mathrm{s}}{\mathrm{m}}$).

The figures on the right hand side show the normalized attenuation of the three surface waves for a chosen frequency. As already mentioned, the true surface wave – the Stoneley wave – ceases to exist in the range of high surface permeabilities α. In the limit value, its attenuation becomes infinite. The remaining two leaky waves possess finite attenuation in the whole range of α.

3.2.4 Group velocities of the three surface waves

For the impermeable boundary ($\alpha = 0$) between a porous material and a fluid we present the group velocities of the surface waves. The group velocity of the leaky Stoneley wave behaves differently from the both waves which also appeared for the boundary porous me-

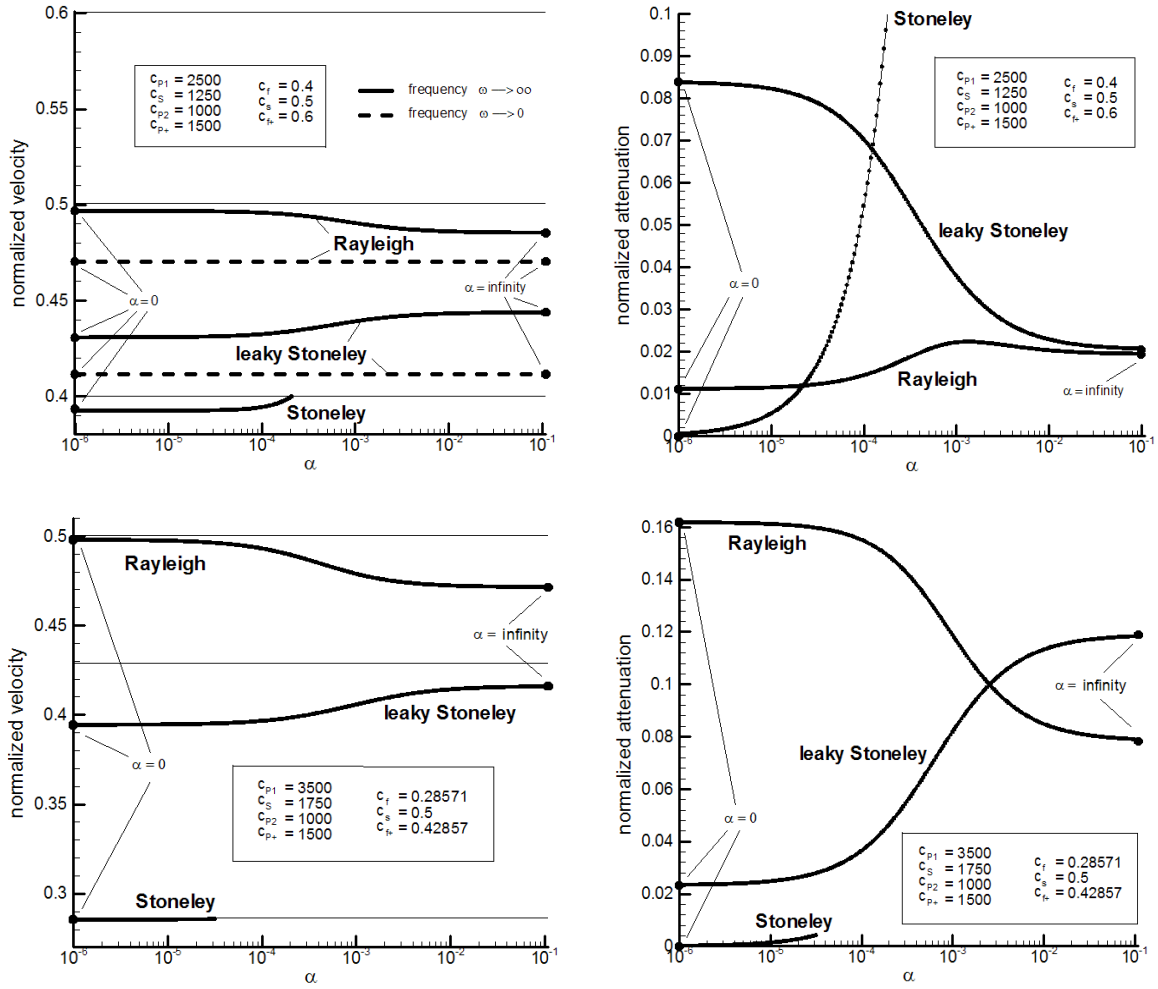

Fig. 18: Normalized phase velocities and attenuations of the three surface waves in dependence on the surface permeability parameter, α, for different material parameters.

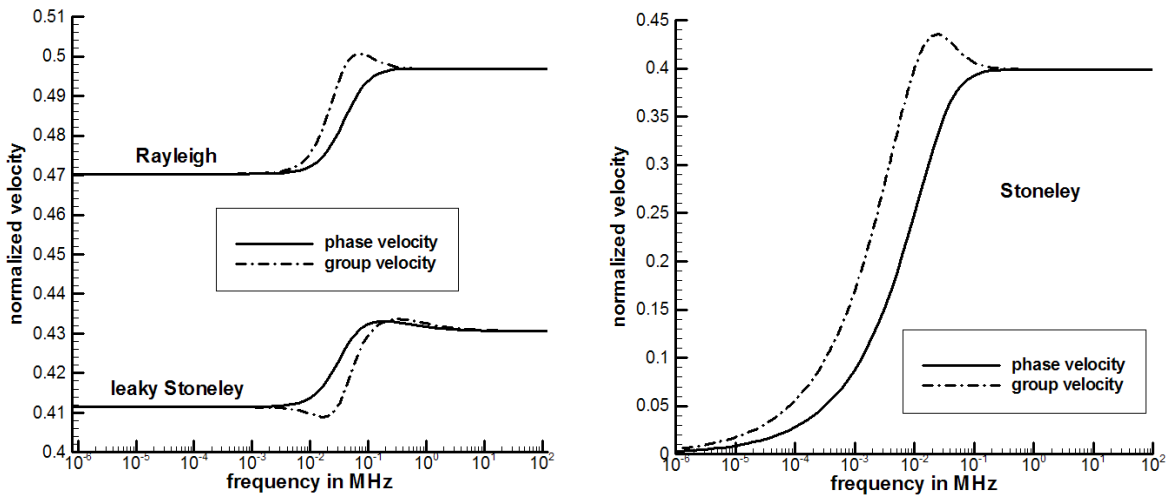

Fig. 19: Normalized phase and group velocities of the three surface waves.

dium/vacuum. While they only possess a maximum for a certain frequency, the leaky Stoneley wave exhibits first a strong minimum and then a slight maximum. The mathematical reason is obvious: the growth in phase velocities of Rayleigh and Stoneley waves is almost monotonous but for the leaky Stoneley wave the phase velocity possesses a clear maximum (compare: Fig. 16), and, as indicated in the box of (42) the group velocity depends on the slope of the phase velocity.

3.2.5 Summary of results for boundary porous medium/fluid

In the whole range of frequencies there exist two leaky surface waves: a leaky Rayleigh wave and a leaky Stoneley wave. In the range of very small values of the surface permeability parameter α, there exists a third true surface wave – a Stoneley wave. The behavior of the Rayleigh wave and the true Stoneley wave in dependence on the frequency is the same as described in Sect. 2.5. Here, we summarize only some additional comments on the α-dependence and on the additional wave appearing at this boundary, the leaky Stoneley wave:

Leaky Rayleigh

- for low frequencies the phase velocity for different values of the surface permeability α remains almost constant. For high frequencies smaller values of α yield bigger velocities; for the open pore case the difference between high and low frequency limits is approx. one half of the difference for a close boundary;
- the attenuation grows linearly and unbounded, there appear singularities which depend on α and seem to be related to the characteristic frequencies $\frac{\pi}{2\rho_0^S}$ and $\frac{\pi}{2\rho_0^F}$;

Leaky Stoneley

- the phase velocity of this wave behaves similarly to this of the leaky Rayleigh wave; however, the high frequency limit is larger for bigger values of α than for smaller ones; a maximum value appears in the region of order 100 kHz; the velocity of the leaky Stoneley wave is for each pair (ω, α) smaller than this of the leaky Rayleigh wave.
- also the attenuation behaves similar to this of the leaky Rayleigh wave; however, the singularities are weaker dependent on α;

Stoneley

- it exists only for small values of the surface permeability α; for different values of α the velocity is nearly the same; it starts from zero and approaches a horizontal asymptote;
- the attenuation of the Stoneley wave grows monotonically to a finite limit for $\omega \to \infty$.

4 Comparison to results of other authors

4.1 Deresiewicz

One of the first attempts to investigate surface waves in two-component porous materials stems from Deresiewicz [14], [15]. In the first of these papers he has studied the boundary porous medium/vacuum using the Biot's equations. He has calculated Rayleigh wave velocities and attenuations. Similar to the procedure of the present article he has found analytical approximations for high and low frequencies and carried out numerical calculations for a kerosene-saturated sandstone. He wrote: "Because of its complexity, the secular (comment by B. A.: dispersion) equation does not lend itself to analytical study for intermediate values of the frequency. Accordingly, a numerical study was undertaken, of the variation of velocity and dissipation per cycle with frequency, for a material whose elastic and dynamical coefficients were available, with several curious results." One of these "curious" results is a minimum of the phase velocity in the region of small frequencies like we found for the Rayleigh wave. However, Deresiewicz located also a second minimum in the range of high frequencies which we did not ascertain. The results for the attenuation, in Deresiewicz's work given as the specific energy loss, are hardly comparable to our results. It is impressing how much the author did know about the Rayleigh wave already in the 60ies. However, it is strange that he did not get the Stoneley solution from the dispersion equation. The second paper concerns surface wave in the presence of a liquid layer. This work is not comparable to our case of a boundary between porous medium/fluid because the liquid layer has a given thickness. Moreover, for this case Deresiewicz only considered low frequencies and did not attain numerical results.

4.2 Feng & Johnson

Feng & Johnson [19] use Biot's theory to search numerically primarily the velocities of various surface waves. They distinguish between the true slow surface wave and the leaky surface waves and calculate their velocities at an interface between a fluid half-space and a half space of a fluid-saturated porous medium like we did in the last section.

They rely on a somewhat different approach to obtain results for the surface waves. Namely, they assume a surface wave to have the characteristic form of being a linear combination of all bulk waves. Under this assumption the displacements can be expressed as

$$\mathbf{u} = \sum_J C_j \widetilde{\mathbf{u}}_j \, \mathrm{e}^{-\gamma_j |z|} \, \mathrm{e}^{i(kx-\omega t)}, \qquad \mathbf{U} = \sum_J C_j \widetilde{\mathbf{U}}_j \, \mathrm{e}^{-\gamma_j |z|} \, \mathrm{e}^{i(kx-\omega t)}, \tag{68}$$

where $\mathbf{u}, \mathbf{U}$ are the displacement vectors of the solid part and the fluid part, respectively. The summation is over the three bulk modes (fast, slow, shear) and $\gamma_j \equiv \left(k^2 - \omega^2/V_j^2\right)^{1/2}$ (V_j are bulk wave speeds). The quantities C_j are the amplitudes of the bulk modes. The polarization vectors for each bulk wave $\left(\widetilde{\mathbf{U}}_j, \widetilde{\mathbf{u}}_j\right)$ are related to each other and to the complex wave vector by requiring the displacements to satisfy the bulk differential equations.

However, in contrast to our approach, Feng &Johnson focus only on the high-frequency range. They also use the boundary conditions introduced by Deresiewicz and Skalak but

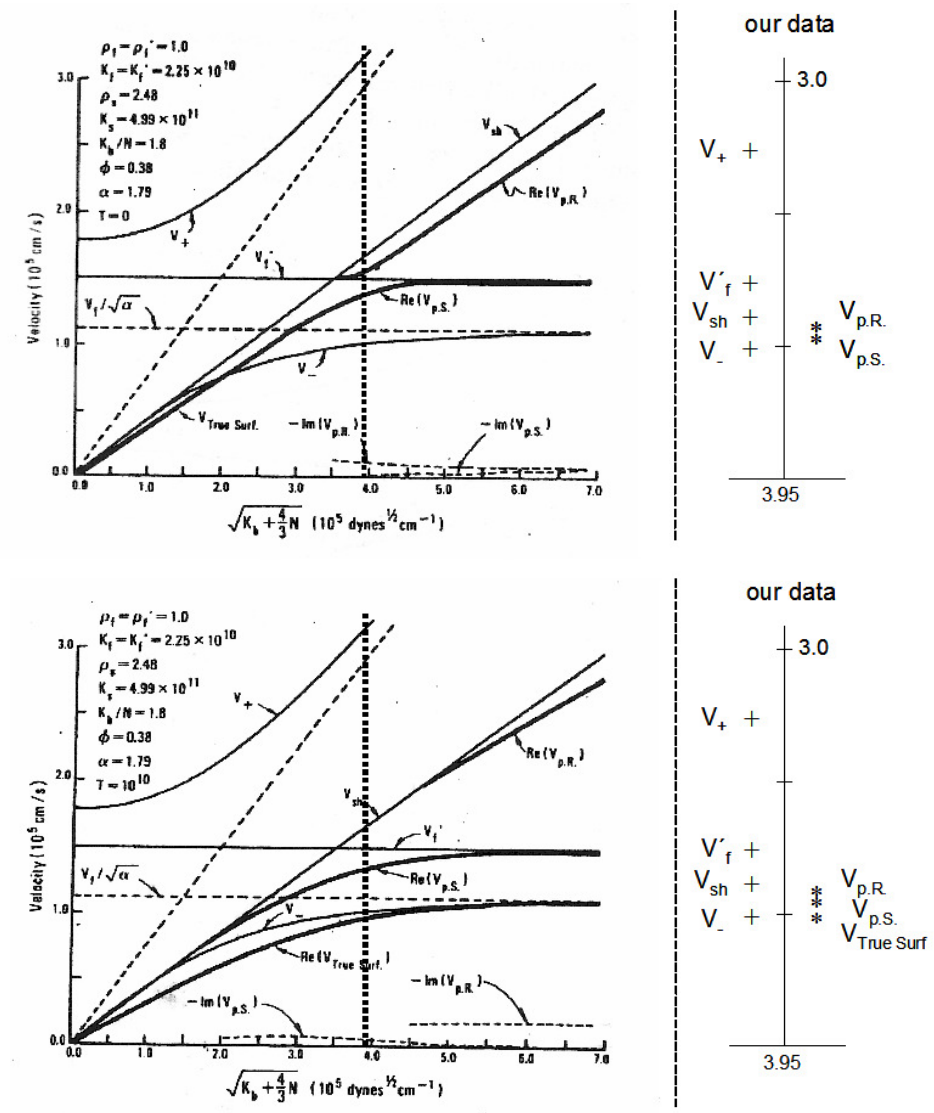

Fig. 20: Figures of the paper by Feng&Johnson [19] for the case: Water as the fluid (in both $z < 0$ and $z > 0$ regions) and fused glass beads as the porous medium extended by a sketch of our results (sandstone instead of glass beads as the porous medium). The points "$+$" and "$\star$" mark the location of corresponding quantities.
At the top: open pore situation, at the bottom: sealed pore situation.

they limit their attention to the open-pore and to the sealed pore situation (i.e. in our notation: $\alpha = \infty$ and $\alpha = 0$, respectively, and in their notation: $T = 0$ and $T = \infty$). In dependence on the stiffness of the skeleton (in their notation: longitudinal modulus of the skeleton frame $\left(K_b + \frac{4}{3}N\right)^{1/2}$, where K_b : bulk modulus of porous drained solid, N : shear modulus of both the drained porous solid and of the composite) and e.g. on the coefficient of added mass ("tortuosity", in their notation: α) they have investigated the existence of the surface modes. We show here some of their numerical results for material parameters which fit best to ours, namely for the case: Water as the fluid (in both $z < 0$ and $z > 0$ regions) and fused glass beads as the porous medium. In order to compare the

results we calculate the stiffness of the sandstone of our example in their notation: With the formula for the longitudinal velocity in the dry sample

$$V_L = \sqrt{\frac{K_b + \frac{4}{3}N}{(1-\phi)\,\rho^{SR}}}, \tag{69}$$

where ϕ : porosity, ρ^{SR} : realistic mass density of the solid, we are able to calculate the quantity appearing as the variable on the horizontal axis

$$\begin{aligned} \sqrt{K_b + \frac{4}{3}N} &= V_L\sqrt{(1-\phi)\,\rho^{SR}} = c_{P1}\sqrt{\rho_0^S} = \\ &= 2500\sqrt{2500}\frac{\sqrt{\mathrm{N}}}{\mathrm{m}} = 125000\frac{\sqrt{\mathrm{N}}}{\mathrm{m}} \approx \\ &\approx 125000\frac{316.23\sqrt{\mathrm{dynes}}}{100\,\mathrm{cm}} \approx 3.9528\cdot 10^5\frac{\sqrt{\mathrm{dynes}}}{\mathrm{cm}}. \end{aligned} \tag{70}$$

Feng & Johnson found that for an open-pore surface situation, the true surface wave exists for a limited range of material parameters and changes continuously into a slightly leaky-Stoneley wave as its velocity crosses over the slowest bulk wave velocity. For the sealed pore situation there exist simultaneously a true surface wave (for all values of material parameters) and a leaky-Stoneley wave. The leaky-Rayleigh wave has features similar to those of the leaky-Rayleigh wave for a fluid/nonporous solid case.

These results are demonstrated in juxtaposition in the following table.

$\frac{\text{vacuum}}{\text{solid}}$	$\frac{\text{fluid}}{\text{solid}}$	$\frac{\text{fluid}}{\text{porous medium}}$
Rayleigh	**leaky-Rayleigh** **Stoneley**	**leaky-Rayleigh** possibly **Stoneley** possibly **leaky-Stoneley** } or both

For the leaky waves the authors claim that "they are roots of the same equation on the wrong Riemann sheet". They explain it as follows: "The pseudo-Stoneley mode has a velocity faster than the slowest bulk mode but slower than the rest of the bulk modes. The pseudo-Rayleigh mode has a velocity faster than the slowest bulk mode and the bulk fluid mode (in the region $z > 0$). These relations imply that these surface modes radiate into the slowest bulk mode (for pseudo-Rayleigh mode: both the slowest and the fluid bulk mode) as they propagate along the surface (i.e. $\mathrm{Im}\left(\gamma_j\right) \neq 0$). Furthermore, the radiation condition requires the radiation of bulk modes to have an exponentially growing factor in the z direction instead of a decaying one; in addition, these pseudosurface modes are attenuated in the x direction, i.e., $\mathrm{Im}\left(V_{\text{ps. surf.}}\right) < 0$. These two physical requirements imply that both $\mathrm{Re}\left(\gamma_{\text{rad. bulk modes}}\right)$ and $\mathrm{Im}\left(\gamma_{\text{rad. bulk modes}}\right)$ are negative. Usually the condition $|\mathrm{Re}\left(\gamma_{\text{rad. bulk modes}}\right)| \ll |\mathrm{Im}\left(\gamma_{\text{rad. bulk modes}}\right)|$ (or $|\mathrm{Im}\left(V_{\text{ps. surf.}}\right)| \ll |\mathrm{Re}\left(V_{\text{ps. surf.}}\right)|$) is satisfied; this corresponds to the situation of "slightly" leaky pseudosurface modes. So in most cases, one can incorporate conditions on the square roots in γ_j's for both the true surface mode and the pseudosurface modes by requiring $\mathrm{Re}\left(\gamma_j\right) - \mathrm{Im}\left(\gamma_j\right) \geq 0$. This treatment of the pseudosurface modes is analogous to the treatment of the pseudo-Rayleigh mode for the fluid/solid case about which there is some controversy [6], [35], [28]."

5 Glance on three-component porous media

Classical soil mechanics and also the classical theory of porous materials are limited to the description of soils and other porous materials which are fully saturated with a fluid (e.g. water or oil). However, there are many practically relevant examples of materials for which such a condition is not fulfilled: their voids are filled partially with a fluid, and partially with a gas – often with vapor – and these possess different partial pressures. Such materials are called "unsaturated" or "partially saturated". In the last 40 years numerous endeavors have been carried out to examine their mechanical behavior (see e.g. [20], [29], [32], [38], [50]) and also the wave propagation in such materials (e.g. [5], [8], [10], [31], [34]).

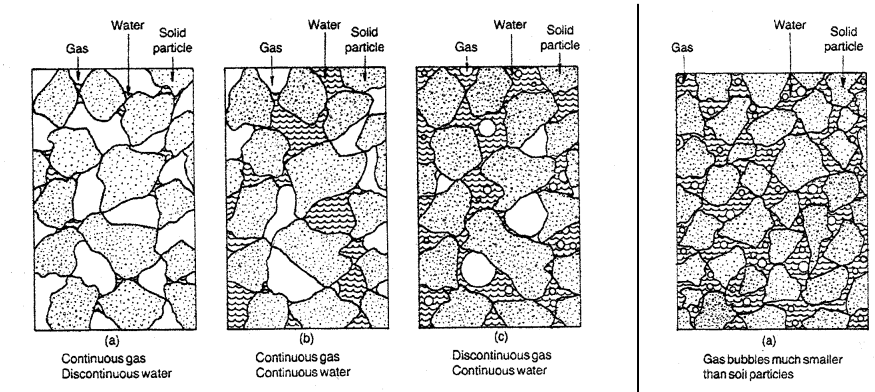

Fig. 21: Classification of unsaturated soils into three groups (left) and the mostly studied case of gas bubbles much smaller than the soil particles; from [38].

It turned out that the basic structure (see Fig. 21) and the acoustic properties of unsaturated media are dependent on the *degree of saturation.* This is the proportion of the fluid volume to the entire volume of voids. Fig. 21 shows a classification of unsaturated soils into three groups and the mostly studied case where the gas bubbles are much smaller than the soil particles.

In contrast to the one-component fluid in the channels of a saturated porous medium the gas fluid mixture contains phase interfaces which affect both the stress state (surface tension) and the flow conditions (e.g. permeability). Additionally, the morphology (e.g. the degree of saturation) is changed permanently by phase transitions, appearance of big gas bubbles instead of some small bubbles etc. In soils, most of the time, the gas occurs in the form of discrete bubbles as shown on the right hand side of Fig. 21. This is the case if the degree of saturation lies above a certain critical degree of saturation which varies for different soils but is of order 85%. For fluid-gas-mixtures mostly it is assumed that the bubbles are spherical. Then the radius of curvature of the gas-fluid interface which determines the surface tension between gas and fluid and thus the difference of pressures in gas and fluid is equal to the radius of the bubble. Also for porous materials there exists an interrelation between size of bubbles, saturation and capillary pressure. An increase of saturation leads also to an increase of the capillary pressure. Hence, for a given radius of bubbles (which can be measured in experiments), there exists a macroscopical relation of the form

$$p_c = p_c\,(S)\,, \tag{71}$$

where p_c denotes the capillary pressure and S the saturation. In the modeling of unsaturated porous materials the form of this relation is one of the most important questions. We do not go into any details here and remark solely that several researchers simply choose a relation from the micro scale. There are also attempts, not yet fully ripe, to create transitions from the micro to the macro scale (e.g. [29]).

A lot of experiments have been performed on the acoustical behavior of unsaturated materials, especially of sediments (e.g. [5]). The experimenters claim that the occurrence of gas bubbles – also in small amounts – has high influence on the acoustic characteristics (propagation velocities, attenuations, reflection etc.). To show this we include here the results of some experiments on sandstone. The figures show the velocity and the attenuation in form of the quality factor of the P1 wave (denoted by E) and the shear wave (S). For small amounts of bubbles (high water saturation) their behavior is particularly strongly dependent on the saturation. Natural sediments contain usually a fraction of gas bubbles between zero and ten percent.

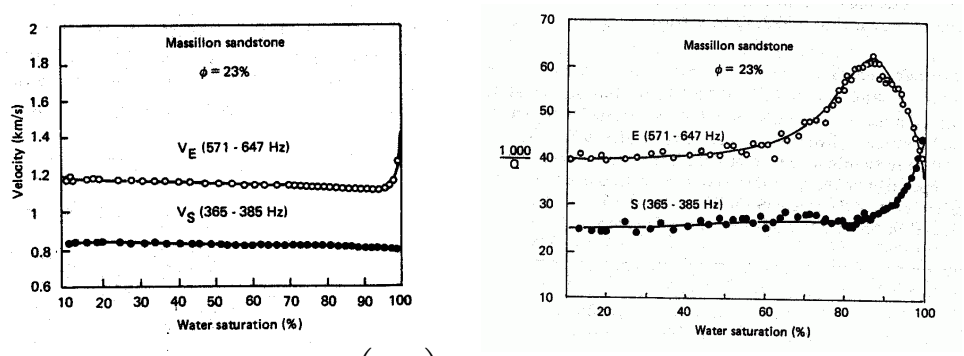

Fig. 22: Velocity and attenuation $\left(\frac{1000}{Q}\right)$ of the P1-wave and the S-wave in sandstone in dependence on the water saturation, experiments by Murphy; from [12].

Helpful for the study of the influence of saturation in porous media may be early works treating the influence of gas bubbles on the sound velocity in pure water. Qualitatively wave velocities in unsaturated sediments should behave like the sound speed in a water-gas-mixture which is given in Fig. 23 (experiments performed by Wood in 1957). We see that there exists an extremely deep minimum in the sound velocity for a certain fraction of air in water.

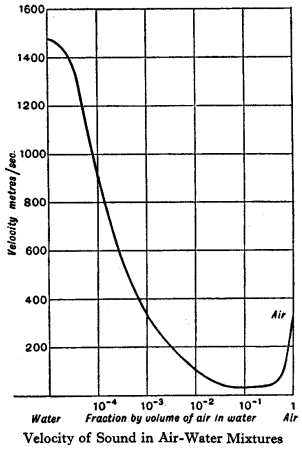

Fig. 23: Sound speed in a water-air-mixture in dependence on the air fraction; from [49]

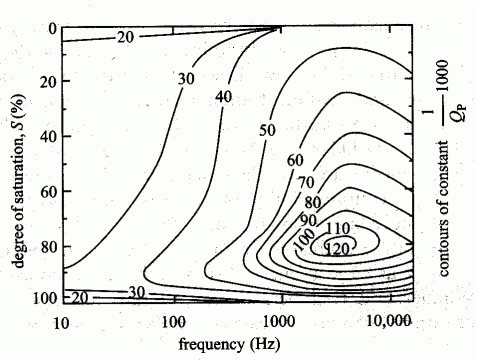

Fig. 24: Influence of the frequency and the saturation on the attenuation of the P1-wave; from [31]

The present article shows that both velocities and attenuations of surface waves (independent of the type of boundary) are highly dependent on the frequency. This is, of course, also true for unsaturated soils. In order to demonstrate this feature Fig. 24 is included which shows the attenuation of the $P1$ wave in dependence on the frequency and on the degree of saturation. We see that the attenuation depends very strong on both parameters.

The above remarks show that even the propagation of bulk waves in unsaturated porous materials has not been investigated yet in this extent as for two-component systems. The investigation of surface waves for such materials does not exist at all. Due to its practical importance such a research direction seems to be a natural continuation of results presented in this article.

References

[1] K. Aki, P. Richards: *Quantitative seismology, theory and methods,* W. H. Freeman and Co. (1980).

[2] B. Albers: Relaxation Analysis and Linear Stability vs. Adsorption in Porous Materials, *Continuum Mech. Thermodyn.*, **15** (2003) 1, 73-95, also WIAS-Preprint Nr. 721, 2002.

[3] B. Albers, K. Wilmanski: On modeling acoustic waves in saturated poroelastic media, submitted to *J.Engn.Mech.*, also WIAS-Preprint No. 874 (2003).

[4] B. Albers, K. Wilmanski: Monochromatic surface waves on impermeable boundaries in two-component poroelastic media, submitted to *Continuum Mech. Thermodyn.*, also WIAS-Preprint No. 862 (2003).

[5] A. L. Anderson, L. D. Hampton: Acoustics of Gas-Bearing Sediments. I. Background, II. Measurements and Models, *J. Acoust. Soc. Am.*, **67**(6), 1865-1898 (1980).

[6] J. H. Ansell: The roots of the Stoneley wave equation for solid-liquid interfaces, *Pure Appl. Geophys.* **94**, 172-188 (1972).

[7] J. Bear, *Dynamics of Fluids in Porous Media,* Dover Publications, New York (1988).

[8] A. Bedford, M. Stern: A Model for Wave Propagation in Gassy Sediments, *J. Acoust. Soc. Am.*, **73(**2), 409-417 (1983).

[9] A. Ben-Menahem, S. J. Singh: *Seismic waves and sources*, Dover (1981).

[10] J. G. Berryman, L. Thigpen, R. C. Y. Chin: Bulk Elastic Wave Propagation in Partially Saturated Porous Solids, *J. Acoust. Soc. Am.,* **84**(1), 360-373 (1988).

[11] M. A. Biot: *Acoustics, elasticity and thermodynamics of porous media: Twenty-one papers by M. A. Biot*, edited by I. Tolstoy, American Institute of Physics (1992).

[12] T. Bourbie, O. Coussy, B. Zinszner: *Acoustics of porous media,* Editions Technip, Paris (1987).

[13] G. Chao, D. M. J. Smeulders, M. E. H. van Dongen: Shock induced borehole waves in porous formations: Theory and experiments, *J. Acoust. Soc. Am.* **116 (**2), (2004).

[14] H. Deresiewicz: The effect of boundaries on wave propagation in a liquid filled porous solid. IV. Surface waves in a half space, *Bull. Seismol. Soc. Am.*, **52**, 627-638 (1962).

[15] H. Deresiewicz: The effect of boundaries on wave propagation in a liquid filled porous solid. VII. Surface waves in a half space in the presence of a liquid layer, *Bull. Seismol. Soc. Am.*, **54**, 425-430 (1964).

[16] H. Deresiewicz, R. Skalak: On uniqueness in dynamic poroelasticity, *Bull. Seismol. Soc. Am.*, **53**, 783-788 (1963).

[17] I. Edelman: Bifurcation of the Biot slow wave in a porous medium, *J. Acoust. Soc. Am.*, **114** (1), 90-97 (2003).

[18] I. Edelman, K. Wilmanski: Asymptotic analysis of surface waves at vacuum/porous medium and liquid/porous medium interfaces, *Cont. Mech. Thermodyn.*, 25-44, **14**, 1 (2002).

[19] S. Feng, D. L. Johnson: High-frequency acoustic properties of a fluid/porous solid interface. I. New surface mode, *J. Acoust. Soc. Am.*, **74**(3), 906-914 (1983), II. The 2D reflection Green's function, *J. Acoust. Soc. Am.*, **74**(3), 915-924 (1983).

[20] D. G. Fredlund, H. Rahardjo: *Soil Mechanics for Unsaturated Soils*, John Wiley & Sons (1993).

[21] P. Hess: Surface acousic waves in materials science, *Physics Today*, March 2002, 42-47 (2002).

[22] H. Kutruff: *Ultrasonics, fundamentals and applications,* Elsevier (1991).

[23] C. Lai: *Simultaneous inversion of Rayleigh phase velocity and attenuation for near-surface site characterization,* PhD-Thesis, Georgia Institute of Technology (1998).

[24] N. G. H. Meyendorf, P. B. Nagy, S. I. Rokhlin (eds.): *Nondestructive Materials Characterization*, Springer Berlin Heidelberg (2004).

[25] P. B. Nagy: Acoustics and ultrasonics, in *Methods in the physics of porous media*, edited by Po-zen Wong, Academic Press (1999), pp.161-221.

[26] A. N. Norris: Stoneley-wave attenuation and dispersion in permeable formations, *Geophysics*, **54**(3), 330-341 (1989).

[27] J. O. Owino, L. J. Jacobs: Attenuation measurements in cement-based materials using laser ultrasonics, *Jour.Engn.Mech.*, **125**(6), 637-647 (1999).

[28] R. A. Phinney: Propagation of leaking interface waves, *Bull. Seismol. Soc. Am.*, **51**(4), 527-555 (1961).

[29] S. Pietruszczak, G.N. Pande: Constitutive Relations for Partially Saturated Soils Containing Gas Inclusions, *Journal of Geotechnical Engineering*, **122**, 1 , 50-59 (1996).

[30] G. J. Rix, C. G. Lai, S. Foti: Simultaneous measurement of surface wave dispersion and attenuation curves, *Geotechnical Testing Journal*, 24(4), 350-358 (2001).

[31] J. C. Santamarina: Soils and Waves, *John Wiley & Sons* (2001).

[32] B. A. Schrefler, L. Simoni, Li Xikui, O. C. Zienkiewicz: *Mechanics of Partially Saturated Porous Media*, in "Numerical Methods and Constitutive Modelling in Geomechanics " (CISM lecture notes), eds. Desai C.S. & Gioda G., 169-209. Springer Verlag, Wien (1990).

[33] C. T. Schröder, W. R. Scott Jr.: On the complex conjugate roots of the Rayleigh equation: The leaky surface wave, *J. Acoust. Soc. Am.,* **110** (6), 2867-2877 (2001).

[34] D. M. J. Smeulders, J. P. M. de la Rosette, M. E. H. van Dongen: Waves in Partially Saturated Porous Media, *Transport in Porous Media*, **9**, 25-37 (1992).

[35] E. Strick: III. The Pseudo-Rayleigh wave, *Philos. Trans. R. Soc.* (London), Ser. A, **251**, 488-522 (1959).

[36] A. Udias: *Principles of Seismology*, Cambridge University Press (1999).

[37] I. A. Viktorov, *Rayleigh and Lamb waves. physical theory and applications,* Plenum Press, New York (1967).

[38] S. J. Wheeler: A Conceptual Model for Soils Containing Large Gas Bubbles, *Géotechnique*, **38**, 389-397 (1988).

[39] J. E. White: *Underground sound. Application of seismic waves*, Elsevier, Amsterdam (1983).

[40] K. Wilmanski: Elastic modelling of surface waves in single and multicomponent systems, in: *Surface Waves in Geomechanics, Direct and Inverse Modelling for Soils and Rocks*, C. Lai, K. Wilmanski (eds.), CISM Courses and Lectures, Springer Wien New York (2004).

[41] K. Wilmanski: Tortuosity and objective relative acceleration in the theory of porous materials, submitted to *Proc. Royal Soc. London, A,* also WIAS-Preprint No. 922 (2004).

[42] K. Wilmanski: Propagation of sound and surface waves in porous materials, in: *Structured media* edited by B. Maruszewski, Poznan University of Technology, Poznan (2002), pp. 312-326.

[43] K. Wilmanski: Some questions on material objectivity arising in models of porous materials, in *Rational continua, classical and new,* edited by M. Brocato, Springer-Verlag, Italia Srl, Milano (2001), pp.149-161.

[44] K. Wilmanski: Waves in porous and granular materials, in: *Kinetic and continuum theories of granular and porous media*, edited by K. Hutter and K. Wilmanski, CISM Courses and Lectures No. 400, Springer Wien New York (1999), pp. 131-186.

[45] K. Wilmanski, B. Albers: Acoustic waves in porous solid-fluid mixtures, in: *Dynamic response of granular and porous materials under large and catastrophic deformations*, edited by K. Hutter and N. Kirchner, Lecture Notes in Applied and Computational Mechanics, Vol.11, Springer, Berlin (2003), pp. 285-314.

[46] K. W. Winkler, H.-L. Liu, D. L. Johnson: Permeability and borehole Stoneley waves: Comparison between experiment and theory, *Geophysics*, **54**(1), 66-75 (1989).

[47] C. J. Wisse, D. M. J. Smeulders, M. E. H. van Dongen, G. Chao: Guided wave modes in porous cylinders: Experimental results, *J. Acoust. Soc. Am.*, **112**(3), 890-895 (2002).

[48] G. B. Whitham: *Linear and nonlinear waves*, John Wiley & Sons, New York (1974).

[49] A. B. Wood: A Textbook of Sound, *G. Bell and Sons*, London (1957).

[50] D. M. Wood: The Behaviour of Partly Saturated Soils: A Review, *Cambridge University Report*, Engineering Department (1979).